



JÖNKÖPING UNIVERSITY
School of Engineering

Doctoral Thesis

Gas Evolution and Transport in Foundry Sands

Dinesh Sundaram

Jönköping University
School of Engineering
Dissertation Series No. 089 • 2024



JÖNKÖPING UNIVERSITY
School of Engineering

Doctoral Thesis

Gas Evolution and Transport in Foundry Sands

Dinesh Sundaram

Jönköping University
School of Engineering
Dissertation Series No. 089 • 2024

Doctoral Thesis in Materials and Manufacturing

Gas Evolution and Transport in Foundry Sands
Dissertation Series No. 089

© 2024 Dinesh Sundaram

Published by
School of Engineering, Jönköping University
P.O. Box 1026
SE-551 11 Jönköping
Tel. +46 36 10 10 00
www.ju.se

Printed by Stema Specialtryck AB 2024

ISBN 978-91-89785-11-3 (Printed version)
ISBN 978-91-89785-12-0 (Online version)



ABSTRACT

Sand-casting is one of the most widely used cost-effective manufacturing techniques to produce metal components for various industries. Constantly evolving environmental regulations have increased the necessity for circular and sustainable manufacturing practices. During the casting process, the mold and core undergo a thermal shock when they come in contact with the molten metal. This triggers a severe reaction due to the evaporation of volatiles and the decomposition of chemical binders. This phenomenon can cause defects such as blow-holes and pinholes, leading to increased scrap. The heat removed from the solidifying melt due to these generated gases also affects the cast component by influencing the mechanical properties. From an ecological perspective, some of the gases generated from the decomposing binders have been identified as environmentally hazardous. Studying the gas generation and transport phenomena during the sand-casting process becomes essential in this context.

In this work, the phenomena that affect heat and mass transport due to the generated gases are studied with the help of newly developed experimental techniques in combination with porous material characterization tools. Combining the experimental data with thermal analysis techniques, a computational model for the heat and mass transport in the foundry core is also developed.

The permeability of the molds and cores plays a significant role in determining how efficiently these gases are transported. The permeability and gas volume affect the pressure build-up and defect formation mechanisms of the mold and core. Traditional measurement methods used for determining permeability are not scientifically comparable, nor can they be used for computing the flow characteristics of the molds and cores. In this work, a custom-made measurement setup to measure the permeability of molds and cores is presented. Using the setup, the effect of variation in the grain size distribution and the density on the permeability is quantified. The results show that density affects the permeability more than the grain size distribution. The samples investigated were also characterized using mercury intrusion porosimetry and X-ray microtomography to study the pore characteristics and pore network of the samples. The existing models to predict permeability were evaluated using experimentally measured values and the obtained pore characteristics. The most suitable model to predict the permeability of foundry cores was identified. The identified model was modified to be able to predict permeability using process parameters.

The gas generation rate and volume vary depending on the production parameters of the molds and cores. Commercially available simulation tools often use simplified models for binder decomposition and gas generation, resulting in reduced accuracy in predicting phenomena pertaining to the sand-casting processes. In this work, a novel method to quantify the gases generated from foundry sand mixtures where the core/mold is subjected to conditions similar to the actual casting process is presented. Along with accurate gas volume data, simultaneous temperature measurements in the central and lateral parts of the sample enabled accurate estimation of the heat absorption characteristics associated with the binder decomposition and the gas generation.

Additionally, thermogravimetry analysis was performed for the Furan binder with several heating rates to study the decomposition characteristics and kinetics. Several possible reactions were identified, and the kinetic parameters for each identified reaction during binder decomposition were computed using the integral method. Using the obtained gas transport properties and the kinetic parameters of the binder decomposition and assuming a local thermal non-equilibrium model for heat transport in the porous material, a computational model was developed for the gas generation and transport process in foundry sand cores/molds. The developed model has been validated to a certain extent based on the experimentally obtained gas volume data. The results of the simulation show that the developed model accurately predicts the rate and volume of gases generated and the pressure build-up in the cores.

Keywords: porous material, mold, core, gas evolution, permeability, binder decomposition, heat absorption, heat transfer, casting defects

SAMMANFATTNING

Sandgjutning är en av de mest använda kostnadseffektiva tillverkningsteknikerna för att producera metallkomponenter för olika industrier. Ständigt föränderliga miljöbestämmelser har ökat behovet av cirkulära och hållbara tillverkningsmetoder. Under gjutningsprocessen genomgår formen och kärnan en termisk chock när de kommer i kontakt med den smälta metallen. Detta utlöser en allvarlig reaktion på grund av avdunstning av flyktiga ämnen och nedbrytning av kemiska bindemedel. Detta fenomen kan orsaka defekter som blåshål och pinnhål, vilket leder till ökat kassation. Ur ett ekologiskt perspektiv har en del av de gaser som genereras från de sönderfallande bindemedlen identifierats som miljöfarliga. Att studera gasgenererings- och transportfenomen under sandgjutningsprocessen blir väsentligt i detta sammanhang.

I detta arbete studeras de fenomen som påverkar värme och gas transport på grund av de genererade gaserna med hjälp av nyutvecklade experimentella tekniker i kombination med verktyg för karakterisering av porösa material. Genom att kombinera experimentella data med termisk analysteknik utvecklas också en beräkningsmodell för värme- och gas transporten i gjuterikärnan.

Formarnas och kärnornas permeabilitet spelar en viktig roll för att avgöra hur effektivt dessa gaser transporteras. Permeabiliteten och gasvolymen påverkar tryckupbyggnaden och defektbildningsmekanismerna i formen och kärnan. Traditionella mätmetoder som används för att bestämma permeabiliteten i formmaterial är inte vetenskapligt jämförbara, och de kan inte heller användas för att beräkna flödesegenskaperna för formarna och kärnorna. I detta arbete presenteras en skraddarsydd mätuppställning för att mäta permeabiliteten hos formar och kärnor. Med hjälp av den nyutvecklade mätuppställningen kvantifieras effekten av variation i kornstorleksfördelningen och densiteten på permeabiliteten. Resultaten visar att densiteten påverkar permeabiliteten mer än kornstorleksfördelningen. De undersökta proverna karakteriserades också med hjälp av porosimetri baserat på kvicksilverinträningar samt röntgenmikrotomografi för att studera poregenskaperna och pornätverket hos proverna. De befintliga modellerna för att förutsäga permeabiliteten utvärderades med hjälp av experimentellt uppmätta värden och de erhållna poregenskaperna. Den mest lämpliga modellen för att förutsäga permeabiliteten hos gjuterikärnor identifierades. Den identifierade modellen modifierades för att kunna förutsäga permeabilitet med hjälp av kända processparametrar.

Genererad gasvolym och dess genereringshastighet varierar beroende på formars och kärnors produktionsparametrar. Kommersiellt tillgängliga simuleringsverktyg använder ofta förenklade modeller för bindemedelsnedbrytning och gasgenerering, vilket resulterar i minskad noggrannhet i att förutsäga fenomen i samband med gjutningsprocesserna. I detta arbete presenteras en ny metod för att kvantifiera de gaser som genereras från sandblandningar som utsätts för liknande förhållanden som kärnor i den faktiska gjutprocessen. Exakt temperaturmätningar i olika delar av experimentella provet möjliggör en noggrann uppskattning av värmeabsorptionsegenskaper förknippade med bindemedlets sönderdelning.

Dessutom utfördes termogravimetri analys för Furan-bindemedlet med flera uppvärmningshastigheter för att studera nedbrytningsegenskaperna och kinetiken. Flera möjliga reaktioner identifierades och de kinetiska parametrarna för varje identifierad reaktion under bindemedelssönderdelning beräknades med användning av integralmetoden. Med hjälp av de erhållna gastransportegenskaperna och de kinetiska parametrarna för bindemedelsnedbrytningen och med antagande av en lokal termisk icke-jämviktsmodell för värmetransport i det porösa materialet, utvecklades en beräkningsmodell för gasgenerering och transportprocess i gjuterisandkärnor/formar. Den utvecklade modellen har till viss del validerats utifrån de experimentellt erhållna gasvolymdata. Resultaten av simuleringen visar att den utvecklade modellen förutsäger exakt hastigheten och volymen av gaser som genereras samt tryckuppbyggnaden i kärnorna.

ACKNOWLEDGEMENTS

I would like to thank my principal supervisor, Professor Attila Diószegi, for trusting, supporting, and guiding me throughout this journey. I am grateful to have gotten the opportunity to learn from your scientific and professional experience. I highly value the time and effort you spent guiding and supporting me. The discussions in your office have always been insightful and reassuring.

I thank my co-supervisors, Associate Professor. Iliia Belov and Associate Professor. Taishi Matsushita. Thank you for your time and meticulous efforts in shaping the thesis to its current form.

I thank my former co-supervisors, Dr. József Tamás Svidró and Dr. Judit Svidró, for your knowledge, support, and guidance. Thank you for trusting and constantly motivating me during the formative years of this journey.

I thank Dr. Vasile Lucian Diaconu for the experimental support and Jacob Steggo for the support in the development of the permeability experimental setup and guidance with thermal analysis tools. Without your time, knowledge, and guidance, this thesis would not have reached completion. I also would like to thank the members of the Lean Cast and Innovative Foundry Technology projects for the productive discussions and valuable contributions to the work.

I thank Professor Peter Leisner for being a kind and supportive manager. Thank you for creating an excellent work environment. I thank Professor Anders Jarfors for his insights and inspiring lectures.

I would like to thank my fellow PhD students and colleagues at the Department of Materials and Manufacturing for being kind and supportive and for creating a conducive work environment.

I would like to thank my master's thesis supervisor, Dr. Pål Schmidt. Without your support, I would not have been able to finish my master's degree and pursue a doctoral degree.

I would like to thank my parents for believing in, supporting, and motivating me. Without your prayers and blessings, this would not have been possible.

I would like to thank my wife for constantly supporting and motivating me. Thank you also for always being there for me. Appa, Amma, and you mean the world to me.

I thank my brother and grandfather for constantly showering their love and blessings.

Dinesh Sundaram
September, 2024

SUPPLEMENTS

The following supplements constitute the basis of this thesis:

Supplement I Sundaram, D., Svidró, J. T., Diószegi, A. & Svidró, J. (2021). Measurement of Darcian Permeability of foundry sand mixtures. *International Journal of Cast Metals Research*, 34(2), 97-103.

<https://doi.org/10.1080/13640461.2021.1917890>

Dinesh Sundaram designed and performed the experiments, analyzed the results, and wrote the original paper draft. Attila Diószegi, József Tamás Svidró, and Judit Svidró contributed with guidance on experimental design, advice on analysis of the data, and review of the paper.

Supplement II Sundaram, D., Svidró, J. T., Svidró, J. & Diószegi, A. (2021). On the Relation between the Gas-Permeability and the Pore Characteristics of Furan Sand. *Materials*, 14(14), 3803.

<https://doi.org/10.3390/ma14143803>

Dinesh Sundaram designed and performed the experiments, analyzed the results, and wrote the original paper draft. Attila Diószegi, József Tamás Svidró, and Judit Svidró contributed with guidance on experimental design, advice on analysis of the data, and review of the paper.

Supplement III Sundaram, D., Svidró, J. T., Svidró, J. & Diószegi, A. (2022). A Novel Approach to Quantifying the Effect of the Density of Sand Cores on Their Gas Permeability. *Journal of Casting & Materials Engineering*, 6(2).

<https://doi.org/10.7494/jcme.2022.6.2.33>

Dinesh Sundaram designed and performed the experiments, analyzed the results, and wrote the original paper draft. Attila Diószegi, József Tamás Svidró, and Judit Svidró contributed with guidance on experimental design, advice on analysis of the data, and review of the paper.

Supplement IV Sundaram, D., Matsushita, T., Belov, I. & Diószegi, A. (2024). Evaluation of Permeability Models for Foundry Molds and Cores in Sand Casting Processes. *Archives of Foundry Engineering*, 24(1)

<https://doi.org/10.24425/afe.2024.149256>

Dinesh Sundaram designed and performed the experiments, analyzed the results, and wrote the original paper draft. Taishi Matsushita, Ilia Belov, and Attila Diószegi contributed with guidance on experimental design, advice on data analysis, and review of the paper.

Supplement V

Sundaram, D., Svidró, J. T. & Diószegi, A. (2024). Thermal analysis and Gas Generation measurement of foundry sand mixtures. *International Journal of Metalcasting*

<https://doi.org/10.1007/s40962-024-01417-2>

József Tamás Svidró and Dinesh Sundaram designed the experimental setup. Dinesh Sundaram and József Tamás Svidró performed the experiments. Dinesh Sundaram and Attila Diószegi wrote the original paper draft and analyzed the results. Attila Diószegi also contributed with guidance on experimental design and advice on the work.

Supplement VI

Matsushita, T., Sundaram, D., Belov, I. & Diószegi, A. (2024). Kinetic model for the decomposition rate of the binder in a foundry sand application. *Archives of Foundry Engineering*

<https://doi.org/10.24425/afe.2024.151289>

Taishi Matsushita was the main author. Dinesh Sundaram and Ilia Belov contributed the original paper draft and analysis of the results. Attila Diószegi contributed with guidance and advice on the work.

Supplement VII

Sundaram, D., Belov, I., Matsushita, T. & Diószegi, A. (2024). Computational model of heat and gas transport in a furan resin sand casting core

Submission ready version

Dinesh Sundaram performed the experiments needed to develop and validate the models and contributed to the original paper draft. Ilia Belov performed the simulations, contributed with the models, the original paper draft, and analysis of the results. Taishi Matsushita contributed to the input parameters/models needed for the simulations and analysis of the results. Attila Diószegi contributed with conceptualization, guidance and advice on the work.

TABLE OF CONTENTS

CHAPTER 1 INTRODUCTION	1
1.1 BACKGROUND	1
1.2 GAS EVOLUTION	2
1.3 MOLDING MATERIALS	3
1.3.1 Aggregates	3
1.3.2 Grain size distribution	4
1.3.3 Grain shape	5
1.3.4 Binder systems	6
1.4 GAS EVOLUTION MEASUREMENTS	7
1.4.1 Traditional methods to measure the amount of gases	7
1.4.2 Alternative methods for quantifying the gas evolution from molding mixtures	8
1.5 GAS PERMEABILITY	10
1.5.1 Porosity	11
1.5.2 Pore size distribution and pore diameter	13
1.5.3 Permeability modeling	14
1.6 MODELING THE HEAT AND GAS TRANSPORT IN THE SAND CORE/MOLD	15
1.6.1 Heat transfer in sand mold/cores	16
1.6.2 Kinetics of binder decomposition	16
1.7 KNOWLEDGE GAPS	18
CHAPTER 2 RESEARCH METHODOLOGY	19
2.1 PURPOSE AND AIM	19
2.2 RESEARCH DESIGN	19
2.2.1 Research perspective and approach	19
2.2.2 Research questions	20
2.2.3 Scope and delimitations	20
2.2.4 Research strategy	21
2.2.5 Overview of the work	21
2.3 MATERIALS AND METHODS	22
2.3.1 Materials	22
2.3.2 Experimental Setup	25
2.3.3 Material characterization	28
2.3.4 Modeling the heat and gas transport in sand core/mold	30
CHAPTER 3 SUMMARY OF RESULTS AND DISCUSSION	31
3.1 GAS TRANSPORT	31
3.1.1 Permeability	31
3.1.2 Pore structure characterization	34
3.2 GAS GENERATION (SUPPLEMENT V)	38
3.2.1 Raw data of gas generation and temperature	38
3.2.2 Thermal analysis	39
3.2.3 Gas generation kinetics	40
3.3 MODELING OF HEAT AND GAS TRANSPORT	41
3.3.1 Kinetic model for binder decomposition (supplement VI)	41
3.3.2 Computational modeling of heat and gas transport in sand mold/core (supplement VII)	43
CHAPTER 4 CONCLUSIONS	45
CHAPTER 5 FUTURE WORK	47
APPENDED PAPERS	57

CHAPTER I

INTRODUCTION

1.1 BACKGROUND

Metal casting is one of the most widely used manufacturing processes for producing metal components, with more than 112 million tons of global production annually catering to several sectors, such as construction engineering, mechanical engineering, and the automotive industry [1]. The sand-casting process is one of the oldest casting processes and was recorded in the classical metallurgical book published in 1540 [2]. Sand-casting is a versatile process that can be used for most of the metals/alloys (both ferrous and non-ferrous). An illustration of the process is provided in Figure 1.1.

The ability to cast complex shapes, high scalability, ability to cast thin sections, and wide production range make sand-casting a preferred route for many industries. It is the only suitable process for several high melting-point alloys, such as steel or cast iron [3]. However, the disadvantages of the sand-casting process are that, for increased productivity, significant investments in the form of automated mold/core-making machinery are needed. Also, the cooling rates are generally low, leading to a coarse grain structure and eventually resulting in inferior mechanical properties. However, due to its advantages, large powertrain components are usually produced using sand-casting.

Molds are prepared using patterns to create a negative impression of the shape of the component that needs to be cast. Cores are added to the molds in cases where the cast component needs internal cavities, contours, or passages in the geometry of the casting. Molten metal is poured onto the molds, where it solidifies. After the solidified metal is cooled to lower temperatures, the sand mold is broken, which is why the process is one of the expendable mold processes used in metal casting. Foundries reclaim the used sand using two major techniques, thermal reclamation, and mechanical reclamation, such that the reclaimed sand is used for further cycles. The percentage of reclamation and reuse of sand differ based on the processing parameters such as aggregate, binder, additives used, alloy cast, and other processing conditions [4,5].

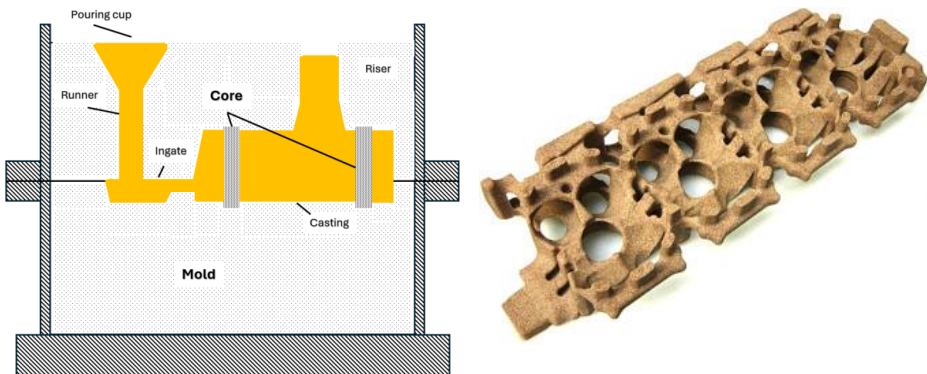


Figure 1.1. An illustration of the sand casting process (a). chemically bonded water jacket core used to manufacture cylinder heads (b) [6].

1.2 GAS EVOLUTION

During the sand casting process, the properties of the mold/core, the interaction between the mold/core and the metal, gases evolving during the process, and the solidifying melt make the mold-metal interface a complex atmosphere. When the parameters involved are not well controlled or studied, defects or undesired properties in the cast component are identified. Porosities, skin defects, defects due to thermal expansion of silica grains, inclusions, etc., can occur [7]. Therefore, the quality of the molds and cores is monitored routinely to ensure they possess optimum properties [8]. Apart from these parameters, the design of the casting system, including the runner and the gating system, influences the soundness of the casting.

When the molten metal comes in contact with the molding materials, due to the high temperature difference, the molding materials undergo a thermal shock, triggering the vaporization of moisture and the decomposition of binders that hold the sand grains together. A large amount of gases are generated during this process [9]. The expanding air in between the sand grains, volatile additives, moisture and decomposing binder contribute to the total volume of gases generated. Along with the porous sand medium, vents and core-prints typically act as the escape route for these gases [10]. When there is a large amount of these gases generated and very little time and/or space for them to escape, these gases enter into the solidifying melt, resulting in defects in the cast component. Winardi et. al. proposed the mechanism behind the gas-related defect formation. In their work, they show that the interaction between the core-gas pressure and the metallostatic pressure dictates the propensity to defect formation. The pressure build-up in the cores when the gases are generated is defined as the core-gas pressure [11]. They show that during the casting, when the core-gas pressure is higher than the metallostatic pressure at a certain point in time, the propensity to gas-related defects is high [12].

Gas-related defects are one of the primary causes of rejections and scrap formation in the foundry industry, resulting in increased material and energy needs for the foundry industry. A thorough understanding of the mechanism behind such defects and the factors influencing these defects will aid in the sustainable manufacturing of metal components through the metal casting route. Apart from defects, some binder formulations used in the foundry industry may release toxic gases such as BTEX (Benzene, Toluene, Ethylxylene, and Xylene), PAH (Polycyclic Aromatic Hydrocarbons), CO₂, H₂S, SO₂, and several other that are considered hazardous from an environmental standpoint.

Simulation tools to model the sand-casting process provide a good overview of the effect of process parameters, the ensuing material properties, and the propensity to defect formation. Most simulation tools focus on models pertaining to the metal domain and lack accurate models for the sand/molding-material domain. In some cases, the thermophysical properties used are not accurate. These simulation tools often lack relevant models to simulate critical phenomena associated with the molding material and sand domain.

In this context, studying and being able to accurately simulate the gas evolution and transport phenomena from molding mixtures becomes vital, and this thesis aims to do that.

1.3 MOLDING MATERIALS

Molding materials used in sand-casting consist of aggregate sand grains of different types that are held together using a binding system (or using pressure in some cases like vacuum casting). Depending on the binding system, they can be broadly classified into physically and chemically bonded sand [13]. Physically bonded sand refers to the green sand molds that constitute sand grains, bentonite, water, and additives. This mixture is bonded together by applying compaction/compression forces. Green sand molding can be classified depending on the type of mold (flask or flaskless) or the machinery used (jolt-type, jolt squeeze, match-plate, pressure wave, etc). Green sand mold is advantageous economically and can yield a high production rate with automated processes [14].

Chemically bonded sand constitutes sand grains, resin, curing agent/catalyst, and/or additives. The resin and the curing agent are called binder systems. They are mainly classified based on the type of curing process employed: gas-cured, self-setting (no-bake), thermo-setting, or drying. Each of these processes uses a different type of binder system [13,15,16]. Chemically bonded sand, especially no-bake sand, is sometimes used for mold-making, too. No-bake sand is used for molds for its dimensional tolerance due to its superior rigidity and mold strength. However, primarily, molds are prepared using green sand processes, and chemically bonded sand is used for core-making [17].

The molding materials are a class of porous consolidated materials where the solid phases consist of the aggregates and the binder system that holds the sand grains together. The flow through porous media is affected by several factors related to the micro and macro structure of the porous media, such as porosity, pore size distribution, density, and permeability [18].

1.3.1 Aggregates

Aggregates used in the sand-casting process refer to the granular particles. Silica sand (SiO_2) is the primary material used for foundry purposes (Figure 1.2). Other types of sand used for foundry purposes include Zircon (zirconium silicate, $\text{ZrO}_2 \cdot \text{SiO}_2$), Olivine (magnesium/iron silicate, $\text{Mg}_2 \cdot \text{SiO}_4$ and Fe_2SiO_4), Chromite (FeCr_2O_4), Aluminium silicate (Al_2SiO_5) [19]. An artificial ceramic from aluminum silicate called mullite is also used to prepare molds and cores. Each of these different types of aggregates has specific properties that affect the quality of the casting. The most important properties of the aggregates are composition, grain shape, grain size distribution, and thermal expansion coefficient [19,20]. The properties of the grains that directly influence the gas evacuation phenomena are discussed below since gas transport is the focus of this work.

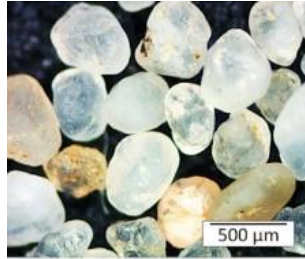


Figure 1.2 Silica sand grains [6]

1.3.2 Grain size distribution

Optimum grain size distribution directly influences the quality of the casting. The size determines the surface area of the grains, influencing the amount of binder needed to obtain the optimum strength. An increase in surface area results in an increase in the amount of resin required. Finer grains in a mold/core result in a lower permeability but improve the surface quality by decreasing the surface roughness. On the other hand, coarser-grained molds have high permeability, but the surface roughness of the resulting casting would be higher. Hence, this trade-off between the finer grains and good surface finish highlights the importance of optimum grain size distribution. Apart from the influence of the casting, the grain size distribution affects the flowability of the sand during mold preparation [21].

Grain size distribution is traditionally measured using the sieve analysis technique, in which the weight of the sand is passed through sieves of different sizes, and the retained sand in each sieve is then calculated in percentiles using multipliers [19]. Typical results of a sieve analysis are provided in Figure 1.3. The sieve sizes are plotted on the x-axis, and the percentage of sand retained in the y-axis. The drawback, however, with this traditional method is that the grains that fall in the range between two sieve sizes are counted in the upcoming smaller sieve. This results in a less accurate estimation of the grain size distribution. During the calculations, multipliers are used to compute the average grain size or the fineness number. It is also to be noted that various grain size distributions can result in the same average grain size values. Nevertheless, the sieve analysis technique reasonably approximates the grain size distribution and the average grain size.

Other modern and more accurate techniques to quantify the grain size distribution of the granular particles currently employed are laser particle size analysis, optical point counting, 2D automated image analysis, and X-ray microtomography [22,23]. Comparison of these methods shows that X-ray microtomography is the most accurate method for particle size analysis for consolidated media [22]. Particle size distribution and the average grain size or, more importantly, the most representative grain diameter (effective diameter) are critical to approximate the flow properties of the mold/core. Grain/particle size distributions can be length-based, surface area-based, or volume based. Depending on the shape and size distribution of the grains, the effective diameter can be determined using these measures [24].

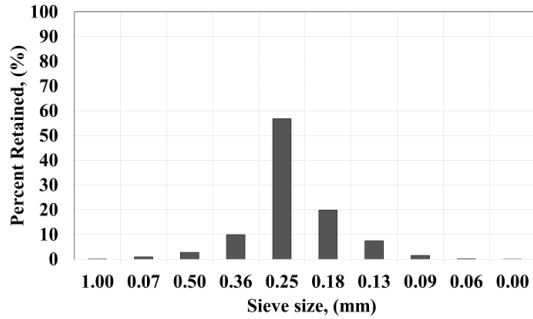


Figure 1.3 Typical sieve analysis results of foundry sands [6]

The distributions typically seen in foundry sands are not Gaussian or normal. They are often found to be skewed to the right. The result of a skewed distribution is that the mean and the median would differ. Therefore, the fineness or effective diameter needs careful evaluation depending on the intended outcome [21]. The fineness or effective diameter could be better represented by the median or D50, which can be computed from the cumulative size distribution plots. For foundry sands, since the shape of the grains is sub-angular, a length-based diameter would be sufficient to represent the distribution accurately.

1.3.3 Grain shape

Grain shape is another critical parameter for foundry sands since it determines the flow characteristics of the molds/cores and the quality of castings. The grain shape, similar to the grain size distribution, determines the amount of binder required for the molds and cores and the permeability or density of the mold/cores. The more rounded, the lesser the specific surface area (surface-to-volume ratio), and vice versa [25]. Generally, foundry sand is said to possess a sub-angular to rounded grain shape [19,25]. Grain shape is determined using microscopic analysis of the sand grains. Modern techniques for particle analysis, such as dynamic light scattering, dynamic image analysis, laser diffraction, or X-ray microtomography, are also employed to determine the shape of the grains. These tools offer better results in determining accurate shape factors of sand grains [26,27]. Figure 1.4 shows the classification of grain shape based on sphericity and roundness.

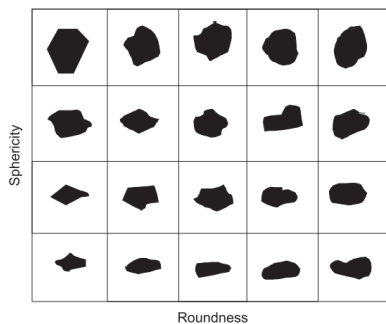


Figure 1.4 Classification of shape factors for determination of grain shape [28].

1.3.4 Binder systems

Green sand systems do not use resins or catalysts to bond the sand grains. Instead, bentonite and water are added, and the mixture is physically compressed to form the mold. On the other hand, chemically bonded systems use resins together with catalysts or other curing systems. Figure 1.5 shows the available binder systems for making molds and cores.

During the core-making process, the resin is added to the sand grains (roughly 0.8 wt. % to 1.6 wt. % with respect to sand). Additionally, for self-setting processes, a liquid acid-based catalyst is added to this mixture (40 wt. % with respect to resin). The type of acid catalyst depends on the resin used (for example – sulphonic acid for Furan resins). A reactive gas is added to the mixture to complete the curing process (sulfur dioxide, SiO₂) for the gas-cured systems. For thermoset resins, heat acts as the curing agent, and in some inorganic binder systems, microwave drying or hot air drying is employed [29].

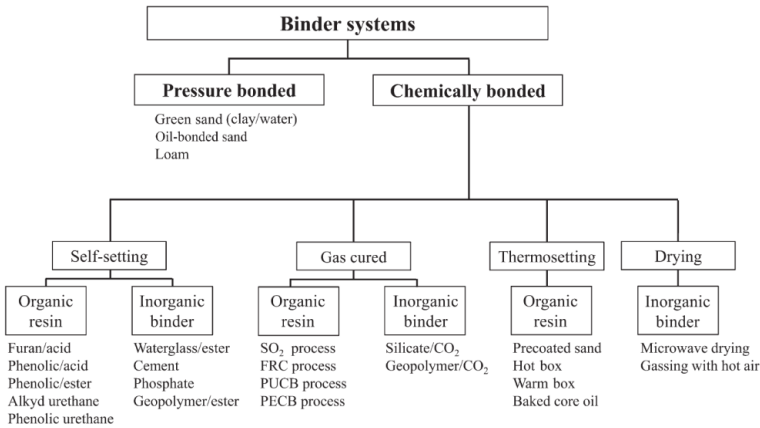


Figure 1.5 The different binder systems for preparing molds and cores [13].

A curing process can be employed for specific binder systems, resulting in polymerization. The resulting polymer could be a thermoset (for example, epoxy resin) or a thermoplastic polymer (for example, polyurethane resin). Hence, during the casting process, the degradation behavior of such polymers will be critical in determining the type of degradation, volume, and rate of gas evolution from such systems. The polymerized resin that holds the sand grains together can be seen in the X-ray microtomography and SEM images in Figure 1.6.

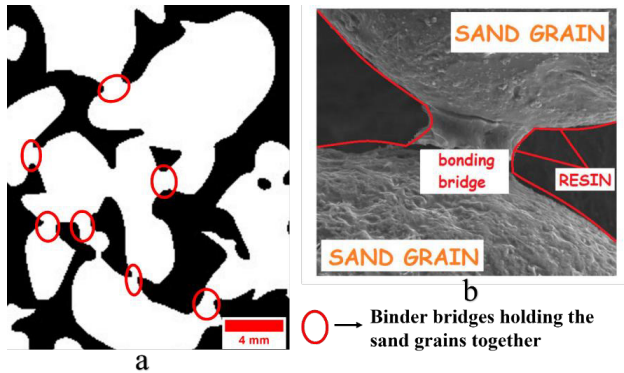


Figure 1.6 X-ray microtomography images of the binder bridges holding the sand grains together, where the black region refers to the porous regions. (a). Scanning electron microscope image showing a binder bridge [30].

1.4 GAS EVOLUTION MEASUREMENTS

Quantification of the gas volume from different binder systems and molding mixtures becomes essential as this data will be crucial in choosing the production parameters during the casting process, such as the type and quantity of the binder system and other properties of the mold/core. Researchers and foundrymen have tried to quantify the volume of evolving gases using traditional methods and custom-made experimental setups.

1.4.1 Traditional methods to measure the amount of gases

An important method to study the decomposition behavior and gas evolution is thermogravimetric analysis (TGA), which measures the amount and rate of change of weight of a material as a function of temperature or time in a controlled atmosphere [31]. Several researchers have widely used TG in foundry technology, mainly to study the decomposition of different binder systems [30,32–37]. Acharya et al. worked on furan binder decomposition and identified the reaction gases using Fourier transform infrared spectroscopy (FTIR). In their work, they also estimated the amount of gases released by pyrolysis and concluded that the amount of hazardous gases is less than the permissible levels [38]. Wan et al. studied the decomposition of Furan no-bake samples, phenolic urethane resin, and alkaline phenolic resin binder by performing TGA and differential scanning calorimetry (DSC) measurements on the Furan no-bake binder samples that were ground into smaller pieces. They estimated the activation energies for the different binder systems. Kmita et al. also studied the different decomposition characteristics of a commercially available alkaline phenolic resin binder. The authors report five reactions that were identified during the decomposition, and they also estimate the activation energy (average) for the five reactions [39]. It could be seen that the decomposition characteristics vary slightly for each binder system based on the composition or on the atmosphere (i.e., depending on whether the samples undergo pyrolysis or combustion). Additionally, the influence of the heating rate is important. This implies that the decomposition characteristics are different for different metallic systems (i.e., ferrous

alloys are cast with a significantly higher temperature range, while nonferrous alloys are cast at substantially lower temperatures). Hence, the influence of the thermal gradient between the mold and the molten metal plays a vital role in the decomposition and subsequent gas evolution.

The results shown in Figure 1.7 show the DSC, DTG, and TG curves for a Phenol formaldehyde resin, which is one of the predominantly used commercial binders. The results show that phenolic resins decompose with multiple steps. DSC results show both endothermic and exothermic peaks.

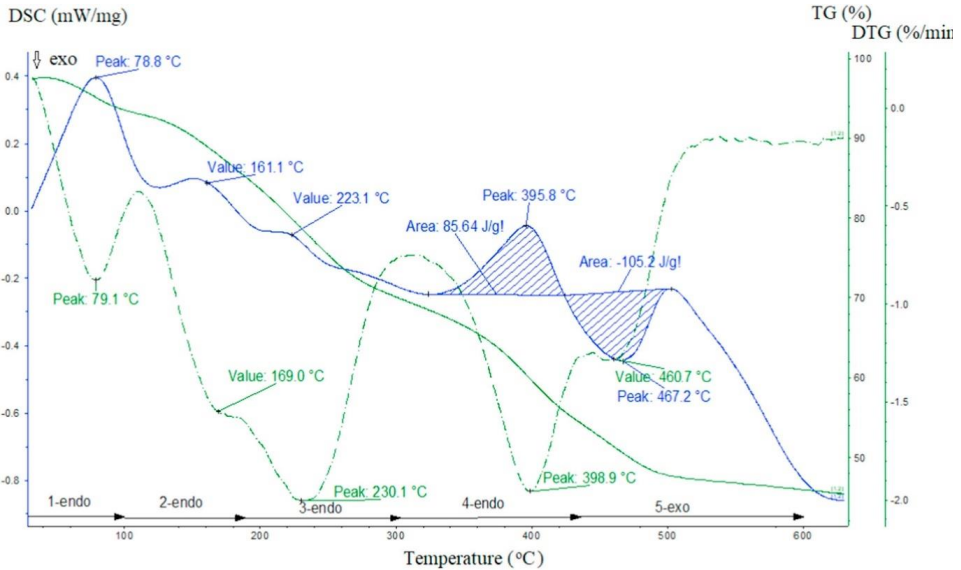


Figure 1.7 The results of the TG, DSC, and DTG measurements of phenol-formaldehyde [40].

Although the traditional methods help calculate critical thermophysical parameters such as the specific heat capacity or estimate the kinetic parameters such as activation energy or pre-exponential factor, there is still a lack of data about the exact influence of the amount of binder on the gas evolution for systems such as furan and phenolic resins. Most of the studies focus on the degradation of the different binder systems and their effect on the environment [41–43]. Also, the heating rates are significantly lower with traditional methods such as TGA and DSC. Therefore, relying on these conventional approaches for quantifying the amount of gases might lead to erroneous conclusions, which led researchers to look for alternative methods to quantify the gas evolution from molding mixtures.

1.4.2 Alternative methods for quantifying the gas evolution from molding mixtures

The need for a database on the quantity of gases evolving from different binder systems will help foundries choose the right type of binder system that leads to the least gas-

related defects. It not only helps to predict defects but also helps to predict the properties of the cast component.

A handful of authors have worked on the gas evolution problem over the past, and recent years [10,38,44–48]. Winardi et al. proposed an empirical equation (Equation 1), including variables such as core permeability and core density [11]. Blow-holes, one of the most detrimental gas-related casting defects, are caused by this pressure build-up inside cores. If the pressure developed in the core exceeds the metallostatic head pressure, then the gases developing in the core can be blown into the melt. Monroe [49], in his work, conducted experiments to verify and confirm this mechanism. Monroe proposed the following empirical equation to estimate the pressure in cores.

$$P = \frac{K(a_c - a_p)V\rho_c C}{a_c P e_{W-N}}$$

Equation 1

where P is the pressure (pa), $K = 0.0185$ is a constant, a_c is the core metal contact area (cm^2), a_p is the total area of the vents or core gas escape area (cm^2), V is the total gas volume per gram of sand (cm^3/g), ρ_c is the core density (g/cm^3), C is the percent of core decomposed (%) and $P e_{W-N}$ is the permeability ($\text{cm}^3/\text{g}/\text{min}$).

Madi et al. studied the effect of varying sand grain size distributions on the gas pressure of foundry cores [50]. They show how the coarse-grained sand cores exhibit less pressure buildup in the cores because of the higher permeability and vice versa.

For pinhole defects, gases enter into the melt in two ways. Firstly, the gases that enter the melt from the decomposition of the molding materials and water vapor present in the mold. Secondly, there is a possibility that the air present in the mold atmosphere can enter into the melt during and after the pouring. From previous research, a possible mechanism for the formation of gas bubbles in the melt that leads to pinhole formation is shown in Equation 2, which shows the mechanism behind the formation of a bubble in the melt [51].

$$P = P_o + \frac{2\sigma}{r}$$

Equation 2

where P is the necessary local gas pressure to form a bubble, P_o is the pressure exerted on the liquid, including atmospheric and metallostatic pressure, σ , surface tension of the melt and r radius of the bubble.

From these models, it could be seen that the pressure prediction depends on the volume of the gases generated from the molding materials, the velocity of gases, and the permeability of the material. The pressure build-up is primarily dependent on the volumetric flow rate of the gases generated and the ability of the molding material to transmit those generated gases (permeability). Hence, it becomes critical to determine the quantity and rate of gases generated from different binder systems to predict the pressure in the cores.

In a recently published work, researchers have developed custom-made measurement equipment to quantify the amount of gases generated from molding mixtures, where they test inorganically bound sand samples. The experimental setup is presented in Figure 1.8. The experimental setup is a combined setup to measure both the gases generated and the permeability of the samples [52]. The setup works based on the principle of condensation of the gases generated. The condensed gases travel through a heated route and eventually undergo condensation when they reach a water reservoir. The increase in the water mass is then estimated and is considered to be the amount of gases generated.

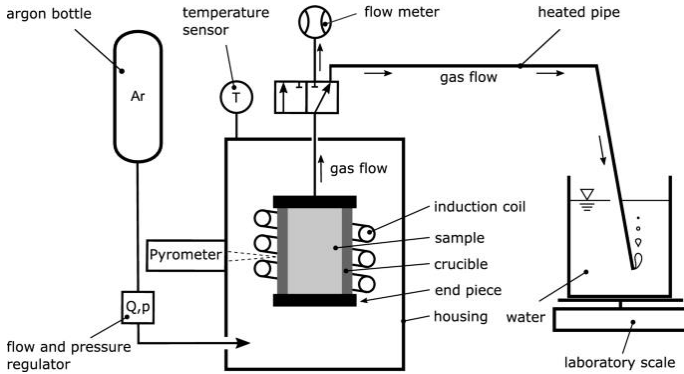


Figure 1.8 An experimental setup used for quantifying the gas evolution from foundry cores [52].

As reported, although a handful of authors have used custom-made instrumental setups or commercially available methods to measure the volume of gas evolving from molds and cores, they do not provide simultaneous measurement of gas evolution and temperature of the molds/cores. Simultaneous temperature measurement would provide the ability to perform thermal analysis during the gas evolution.

Hence, an accurate database of the volume and rate of gas evolution for different binder systems is essential for accurate pressure prediction and developing a robust gas evolution and defect prediction model.

1.5 GAS PERMEABILITY

Gas permeability can be defined as the ability of a material to transmit fluids through it. [53]. Effective removal of volatiles depends on the permeability of the mold/core. Low permeability in the molds and cores leads to gas-related defects. Conversely, significantly higher permeability leads to surface defects due to the nature of the pores in the mold/core. Therefore, an optimum permeability is essential for casting defect-free components [25]. Darcy's law governs the permeability of porous material [54]. Darcy's law is given in Equation 3.

$$Q = \frac{K \cdot A \cdot \nabla p}{\mu \cdot L}$$

Equation 3

where Q is the volumetric flow rate (m^3/s), K is the permeability (m^2), ∇p is the differential pressure (Pa), μ is the dynamic viscosity ($\text{kg}/\text{m}/\text{s}$) and L is the length of the sample measured or simply path length.

For foundry cores and molds, the standard test method for gas-permeability measurement approved by the American Foundry Society results in a dimensionless number called permeability number using parameters [4]. The test procedure applies a modified version of Darcy's law (Equation 4), where the time t a sample takes to let a certain volume of fluid pass through is measured. This permeability number can be used as a comparison tool to determine the differences in permeability between samples.

$$P = \frac{v \cdot h}{p \cdot a \cdot t}$$

Equation 4

where P is the permeability (unitless), v is the volume of air passing through the sample (cm^3), h is the length of the sample (cm), p is the pressure difference between the inlet and the outlet side of the sample (gf/cm^2), a is the cross-sectional area of the sample (cm^2) and t is the time taken for the volume of air to pass through the sample (min).

Apart from the standard technique governed by Equation 4, several other methods or equipment exist to measure the permeability of foundry molds and cores [55–58]. However, these methods do not result in permeability values in standard units and remain as comparative tools to study or compute flow characteristics in the mold. Hence, to compute the flow characteristics of molds and cores, permeability in standard units of m^2 becomes a necessity.

In other fields of research, such as earth sciences or petrophysics, permeability plays a critical role and is measured experimentally to obtain values in standard units [53]. In foundry technology, only a few researchers have measured the permeability in standard units using experimental techniques such as the ones employed in earth sciences. Kumar et al. measured the permeability of ceramic shells used in the investment casting process using the pressure drop technique [59]. A few others have estimated permeability numerically or through simulations [60,61].

Most research in foundry technology has been on the effect of permeability (measured in non-standard units) on pressure build-up, defect formation, or other phenomena. Madi et al. studied the effect of permeability on the gas pressure by varying the resins and casting temperatures [62]. Very little work has been done on the pore characteristics of foundry samples.

1.5.1 Porosity

The micro/macro structure of the porous material influences the permeability [63,64]. The porosity and pore characteristics are affected by factors such as the compaction rate, grain shape, grain size, and the amount of binder used [65,66]. Moreover, since porosity correlates clearly with permeability, studying the porosity and pore characteristics enhances the understanding and computation of the permeability of a porous material [67].

The porosity of a material can be defined as the measure of voids, or more simply, it can be given by the ratio of the solid volume to the total volume of a material [18]. The porosity of a material can be measured with different techniques. Figure 1.9 provides an overview of the available methods depending on the scale of the pores in the material classified by the International Union of Pure and Applied Chemistry IUPAC [68–70].

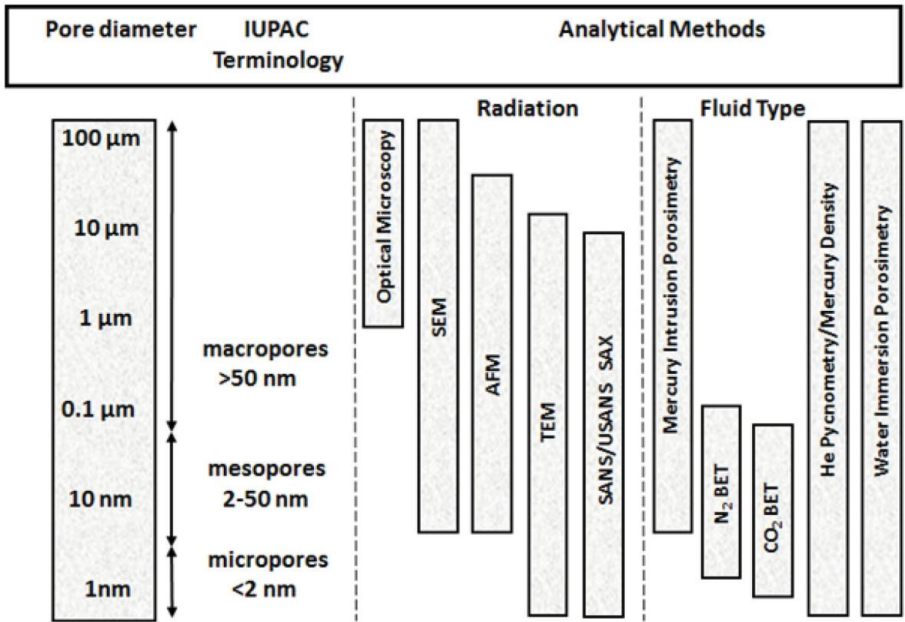


Figure 1.9 The different characterization techniques for measuring the porosity of material depending on the pore sizes [68].

The porosity of foundry cores has not been studied extensively since permeability has been measured in foundries using permimeters. Porosity has, therefore, only been estimated based on direct method estimation based on the apparent density and the true density [71]. The method might provide an approximate estimation of the porosity. A few researchers have used X-ray microtomography technique to estimate the porosity of foundry molds and cores [60,61].

A generic relationship between porosity and permeability has been established for several classes of porous materials. Sandstones of different types have been reported in the literature to show a power-law relationship (Figure 1.10) [72,73]. However, this relationship has been disputed with experimental data for several materials, showing that the power law relationship is insufficient to predict or estimate the permeability for all materials [74].

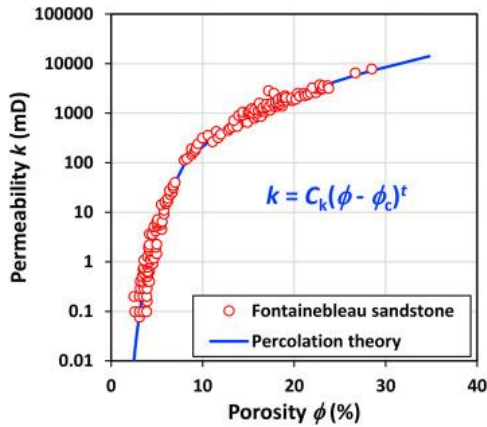


Figure 1.10 Porosity-permeability relationships for sandstones reported in the literature [72,73].

This is due to the complex structure of a porous material. In certain cases, the porosity of two materials could be the same, but they exhibit different permeabilities due to other aspects, such as pore size distribution and pore diameter [67].

1.5.2 Pore size distribution and pore diameter

Quantifying porosity using adsorption techniques, pycnometry, microtomography, and porosimetry provides the ability to also compute the pore size distribution of the material studied [71]. The pore size distribution of a porous material provides information about the sizes and concentration of pores. The amount of pore space present in the material can be directly obtained from the pore size distribution data. A relationship established between the pore size distribution and the permeability has been suggested by Marshal et al. [75].

$$K = \varepsilon^2 n^{-2} [r_1^2 + 3r_2^2 + 5r_3^2 + \dots + (2n - 1)r_n^2] / 8$$

Equation 5

where r is the pore radius (cm) and the subscript of, r, n , corresponds to the corresponding pore number and ε , is the porosity.

The pore size measurement with porosimetry techniques such as mercury intrusion porosimetry (MP) assumes the shape of the pore as cylindrical and follows the Washburn equation (Equation 6), which relates the pressure and size of a pore [76].

$$P = \frac{-2\gamma \cos \theta}{r}$$

Equation 6

where P is the pressure (MPa), γ is the surface tension (interfacial energy) of the mercury (N/m) and θ is the contact angle of mercury with the material (deg).

The pore size distribution has not been characterized extensively for foundry molds and cores. A few authors studied the pore size distribution to model the transport properties of additively manufactured molds and cores [60,61,77]. Manoharan et al. studied the pore characteristics and their effect on permeability (in non-standard units) using mercury intrusion porosimetry [78]. A typical result of the mercury intrusion porosimetry is shown in Figure 1.11. The results of mercury intrusion porosimetry are usually presented in two different forms: cumulative pore volume as a function of pore diameter and differential pore volume as a function of pore volume. The differential pore volume provides crucial information about which pore diameter is predominant in accumulating the intruding mercury.

The critical pore diameter is the smallest diameter of a pore that forms interconnected voids. It is the minimum diameter after which the porous structure is most interconnected (most gases are evacuated through pores larger than this diameter [79–81]).

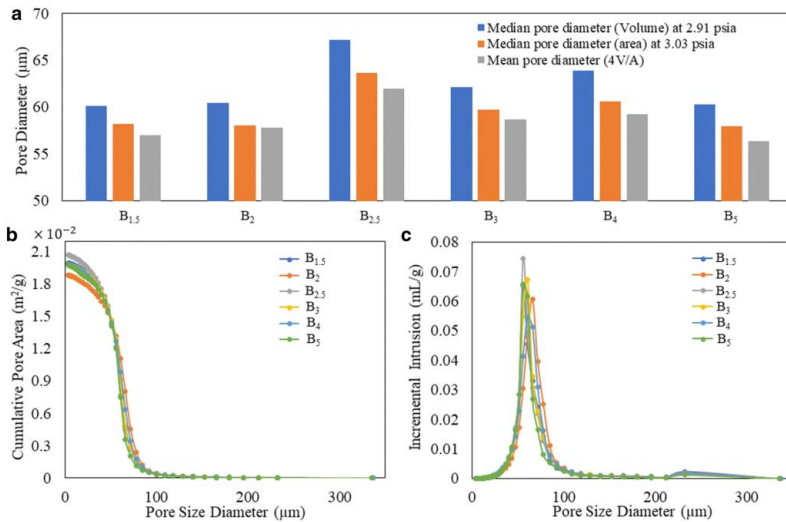


Figure 1.11 The results of mercury intrusion porosimetry data for additively manufactured sand molds [78].

1.5.3 Permeability modeling

Permeability prediction models have been of significant interest for all classes of porous materials. Since measurement of permeability is difficult for several porous materials such as sediments, sandstones, etc, and other materials in several fields [82,83]. Permeability models also help in developing and enhancing the simulation/modeling of heat and mass transport in porous media [18,84,85].

Different types of models have been developed in several fields for this purpose. Machine learning models that use large sets of experimental data [86] are becoming increasingly popular. Traditional theoretical models, such as capillary models, are developed based on the assumption that the material is filled with cylindrical pore capillaries [87]. Fractal

geometry-based models and pore-space based models combined with empirical data are the most common types of models [60,61,67,74,88–90]. Numerous works from researchers across different fields can be identified on this front. The need to revisit these existing models and develop new models arises because of the difficulty of applying these models to different materials.

The pore space models originate from the Dupuit-Forchheimer assumption for fluid flow [87]. Also, due to the bundle of capillaries model assumption, the Navier Stokes equation or the Hagen-Poiseuille equation for each capillary (Equation 7).

$$v = \frac{q}{\varphi}$$

Equation 7

where φ is the porosity, v is the total velocity (m/s) (also known as the Darcian velocity), and q is the local pore velocity (m/s). The Darcian velocity is the average velocity of the fluid passing through a porous medium. The total volume flow, Q , through a capillary is given by the Hagen-Poiseuille equation, shown in Equation 8.

$$Q = \frac{\pi D^4}{128\mu} \cdot \frac{dp}{dx}$$

Equation 8

where D is the diameter of the capillary (m), dp/dx is the pressure gradient across the length of the capillary (Pa), and μ is the viscosity of the fluid (Pa/s).

The basis for several permeability models arises from the Hagen-Poiseuille equation combined with the Darcy law.

In foundry technology, only a few researchers have attempted to predict the permeability of foundry cores and molds. These works primarily used the most widely used pore space model, which is the Kozeny-Carman model. The Kozeny-Carman model has been used specifically for additively manufactured cores [60,77]. A few others have used lattice Boltzman-based models to predict the permeability of foundry molds and cores using X-ray microtomography data and combining it with simulation tools. However, such works do not focus on predicting permeability based on the microstructural parameters such as pore size, grain size, and other characteristics of the porous material [61].

1.6 MODELING THE HEAT AND GAS TRANSPORT IN THE SAND CORE/MOLD

Modeling the heat and gas transport involved in the heat and gas transport involves multiple phenomena acting simultaneously or consecutively. The heat transfer in the porous sand domain, the decomposing binder and the vapourization of the moisture, and the transport phenomena, including the permeability and the velocity of the flowing fluid, make it a complex phenomenon to simulate and model. There have been attempts in the

past to model the phenomena using commercial simulation tools [91,92]. However, these commercial tools assume thermal equilibrium between the solid (sand grains) and the fluid (gases) phases. Such an assumption is made during the modeling because the convective heat transfer in the core due to the release of gases is neglected.

1.6.1 Heat transfer in sand mold/cores

All three modes of heat transfer exist in the sand mold/core during the casting process. Conduction between the sand grains in contact dominates the heat transfer process. However, convection due to the evolving gases contributes to roughly fifteen percent of the overall heat transfer. Although minimal in most cases, radiation from the mold to the outside of the casting also occurs [93,94]. Several studies show that during the sand-casting process, the thermal shock and the accompanying gas evolution act as a convective heat transfer source, and the decomposing binder acts as a significant heat absorption source [93,95]. The heat transfer in the solid phase is given by Equation 9 [18]. Thermal shock and evolving gases create a non-equilibrium atmosphere, and therefore, a local thermal non-equilibrium model for the heat transfer process in sand molds and cores can be given using the following equations [18].

$$(1 - \phi)\rho_s c_{p,s} \frac{\partial T_s}{\partial t} = \nabla \cdot ((1 - \phi)k_s \nabla T_s) + q_{sf}(T_f - T_s)$$

Equation 9

The heat transfer in the fluid phase is given by Equation 10 [18].

$$\phi \rho_f c_{p,f} \frac{\partial T_f}{\partial t} + \phi \rho_f c_{p,f} \mathbf{u}_f \cdot \nabla T_f = \nabla \cdot (\phi k_f \nabla T_f) + q_{sf}(T_s - T_f)$$

Equation 10

where ϕ is the porosity, ρ is the density (kg/m^3), c_p is the specific heat capacity ($\text{J}/(\text{kg}\cdot\text{C})$), \mathbf{u}_f is the fluid velocity vector (m/s), q_{sf} is the interstitial convective heat transfer coefficient ($\text{W}/(\text{m}^2\cdot\text{K})$), k is the thermal conductivity ($\text{W}/(\text{m}\cdot\text{K})$) and T is the temperature (K). The subscripts s and f refers to solid and fluid phases respectively.

1.6.2 Kinetics of binder decomposition

Gas source formulation is critical in establishing a heat and gas transport model for the sand-casting process. As mentioned earlier, the sources of volatiles and gases are moisture and the decomposing binder in the case of cores. The decomposition of the binder can be modeled using polymer degradation mechanisms, which also indicates the thermal stability of the binder [36,96]. Kinetic parameters such as the activation energy and the pre-exponential factor determine the rate of decomposition and the amount of material decomposing at a specific temperature [35,92]. However, the decomposition of polymers in the casting process is driven by a substantial thermal gradient originating from the molten metal. Therefore, the heating rates involved in the process are significant.

Depending on the type of binder, the number of reaction steps differs, and the reaction temperatures vary [39,97]. Traditionally, TG analysis or differential thermal analysis (DTA) is employed to estimate the kinetic parameters based on Equation 11 [98].

$$\frac{dx_g}{dt} = k(1 - x_g)^n$$

Equation 11

where $k = A \exp\left(-\frac{Q}{RT}\right)$, x_g is the fraction of gas (decomposed binder), t is the time (s), n is the order of reaction, Q is the activation energy (J/mol), A is the pre-exponential factor, R is the gas constant, T is the temperature and k is the reaction rate constant.

Thermal analysis studies the relationship between a sample property and its temperature as the sample is heated or cooled in a controlled manner [70]. Thermal analysis is an umbrella term used for several different methods that encompass the study of the properties of a material using its temperature. One important method to study the decomposition behavior and gas evolution is thermogravimetric analysis (TGA), which measures the amount and rate of change of weight of a material as a function of temperature or time in a controlled atmosphere [99].

The setup consists of a furnace, which heats the sample along with the surroundings, and the temperature sensor is placed close to the sample (the position depends on the different types of instruments). The sample holder is placed under a physical balance that accurately measures the mass of the sample. The furnace temperature programmer controls the heating rate, and during the heating, the changes in the mass of the sample are recorded. The changes recorded in the mass during a controlled heating program in a controlled atmosphere will provide information on the changes the material undergoes, including oxidation and decomposition reactions. Depending on the changes the material undergoes, the weight of the sample increases or decreases. Some significant changes that induce a weight change in a material are oxidation, oxidative decomposition, evaporation of volatile substances, etc. [100].

The representation of results is typically presented as mass loss as a function of time or temperature. Alternatively, the percentage of mass loss can also be plotted against time or temperature. The fraction of decomposition can be calculated using the equation below to study the kinetics.

$$\alpha = \frac{m_s - m}{m_s - m_f}$$

Equation 12

where α is the fraction decomposition, m_s is the original mass, m_f is the final mass and m is the mass at any time. The fraction decomposition can then be incorporated into the Arrhenius equation, from which critical decomposition characteristics include the pre-exponential factor and the activation energy.

$$\frac{d\alpha}{dt} = z \cdot \exp\left(\frac{-E_a}{RT}\right) (1 - \alpha)^n$$

Equation 13

where α is the fraction decomposition, z is the pre-exponential factor, E_a is the activation energy, R is the gas constant, T is the temperature and n is the reaction order. The decomposition kinetics of a material can then be estimated.

1.7 KNOWLEDGE GAPS

The literature review identified shortcomings in understanding, quantifying, and modeling the Gas generation and transport phenomena in foundry sands.

- Less focus has been placed on developing and optimizing heat and gas transport models in the sand domain. Although several authors have measured gas evolution data, an experimental setup replicating the casting process is unavailable. Additionally, the volume of gases and the rate of gas evolution as a function of the temperature of the mold/core is lacking. Also, the effect of binder degradation and evolving gases on heat absorption from solidifying melts is lacking. Since the rate and volume of the gases generated at a particular temperature or time critically affect the pressure buildup in the core/mold, it becomes vital to obtain such data.
- The permeability of the mold/core that drives the evacuation of the generated gases is not measured in standard scientific units, which enables the development of gas evolution and transport models. Additionally, the effect of grain size distribution and the density of the mold/core on the permeability in standard units is lacking. In foundry technology, the upper and lower limits of the porosity, density, and grain size distributions of foundry cores are quantifiable, and the effect of these parameters on permeability would be helpful for accurate gas transport models.
- Although several permeability prediction models exist for different materials, an accurate model for foundry molds/cores is lacking. Moreover, a model that considers process parameters relevant to foundry technology will also help determine permeability in local regions of molds and cores. Also, the existing models often use complex parameters that are tedious to measure, creating difficulties for foundries or simulation tools to incorporate permeability prediction.
- Accurate gas generation and transport models that consider the effect of gas generation and evacuation of gases from molds and cores enable better defect and microstructure predictions. The existing models do not treat the heat transfer in molds with a local thermal non-equilibrium approach and do not accurately define the porous media properties such as porosity and permeability. Hence, an accurate model for gas generation would enhance the simulation of the sand-casting process.
- Existing gas generation models formulate the gas source using single effective kinetic parameters such as activation energy or pre-exponential factor [101]. Such approximations of the kinetic parameters for binder degradation might result in underestimating the pressure build-up in the core/mold and inefficient defect predictions.

A robust model that accurately incorporates the gas generation data and accurately defines the gas transport properties of the mold/core can significantly improve the simulation and modeling of the sand-casting process.

RESEARCH METHODOLOGY

CHAPTER INTRODUCTION

This chapter defines the purpose and aim of the research work, the relevant research questions studied, and the research methods employed. Also, an overview of the thesis work is provided, showing how the research questions are addressed and how the supplements aid in answering them.

2.1 PURPOSE AND AIM

The work focuses on developing experimental methodologies to accurately quantify data relevant to understanding the gas generation and transport phenomena in foundry sands such that accurate gas generation and transport models can be developed to simulate the sand-casting process. The work strives to help foundries understand the gas generation problem better by addressing the effect of the relevant parameters, such as the rate and volume of gases generated and the permeability of the molds and cores. The work also focuses on including the effect of process parameters on the transport properties of the mold/core. Therefore, foundries and foundry researchers would benefit from the results of this thesis work. Since the work also aids in the development of accurate simulation models for sand casting, the work also enables sustainable manufacturing of cast components.

2.2 RESEARCH DESIGN

This section discusses the perspective of the research and the research methodologies that help achieve the aim of the work is discussed.

2.2.1 Research perspective and approach

The work performed within the domain of foundry technology encompasses several fields, such as physics, chemistry, and materials engineering. Therefore, the research method used was predominantly experimental in nature. An experimental method/experiment in scientific practice should consist of three essential aspects [102].

- Control of background factors
- Intervention on the target variable by manipulation
- Observation of the result of the intervention

An experimental method should be free from influence problems, interpretation problems, or other errors. An experimental method should be repeatable, reproducible, and also replicable. Experimental control is essential to eliminate background factors. Any experimental method should be operationalized efficiently to observe the desired property using a hypothesized method that is free from bias of any kind [103].

In this work, two different experimental techniques have been developed, considering the requirements for a successful experimental method. Based on the results, the conclusions and generalizations presented in this work can be categorized as inductive inferences. Additionally, the material characterization tools and methods used in this thesis work are well-established experimental techniques. The details about those techniques and their principles are discussed in relevant sections of the thesis. A rigorous literature survey was performed for the method development, and several essential sources from different research fields were duly cited. The results obtained from the experimental measurements were triangulated by verifying the results with other sources, such as relevant models and experimental data from the literature, such that the validity and relevance of the results are upheld [104].

The experiments were designed to avoid experimental artifacts. The method development is elaborated in detail, which ensures research replication and repeatability [104]. In addition to the author of the thesis work, the experiments were performed by several researchers, including master thesis students, to ensure that the experimental method is devoid of experimenter bias. The experiments were performed multiple times for each sample to avoid any chance bias and to ensure the reliability of the results. Apart from these, the chemicals used for the sample preparation were handled by incorporating all the safety aspects. Since certain materials used in the thesis are classified as hazardous elements, they were handled with care, and this was ensured by involving a standard Swedish national research center such that the environmental and safety aspects are considered.

2.2.2 Research questions

The following research questions (RQ) were defined based on the identified knowledge gaps to drive the work toward the intended aims.

RQ.1. How can the rate and amount of gases generated from foundry molds/cores be quantified with proximity to actual casting conditions?

RQ.2. How can the effect of variations in grain size distribution and density on the permeability and pore characteristics of molds/cores be quantified?

RQ.3. How can the existing permeability models be tailored to suit foundry applications?

RQ.4. How can the accuracy of gas generation and transport simulation models for foundry sands be increased?

2.2.3 Scope and delimitations

This thesis studies the relevant phenomena that influence the gas evolution and gas and transport in foundry mixtures. Although the casting system design plays a vital role in the soundness of the casting, aspects relating to the design of the casting are not in the scope of this work. Moreover, the effect of mold/core coating on the permeability is not studied.

2.2.4 Research strategy

The research strategy was structured as shown in Figure 2.1. Within the scope of the work, an extensive literature search was performed to identify the research questions and refine them when needed. The next step was to design and execute suitable experimental procedures, including identifying suitable characterization techniques. The experimental data was then observed and analyzed; additional experiments were performed when needed. Finally, suitable models with the analyzed data were developed. Finally, conclusions from the different steps of the research were drawn.

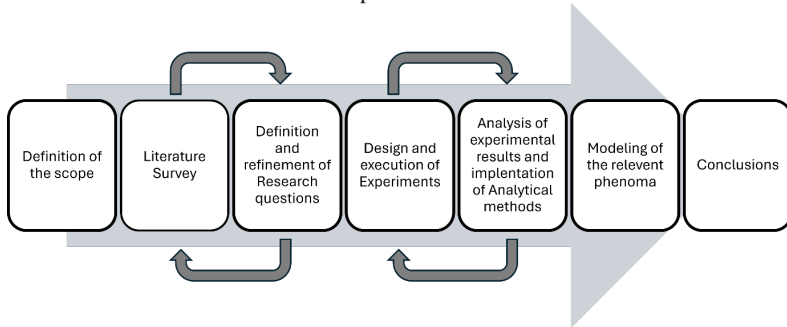


Figure 2.1 The research process/strategy of the work

2.2.5 Overview of the work

The defined research questions were addressed using several supplements. An overview of how the supplements relate to answering specific research questions is shown in Figure 2.2.

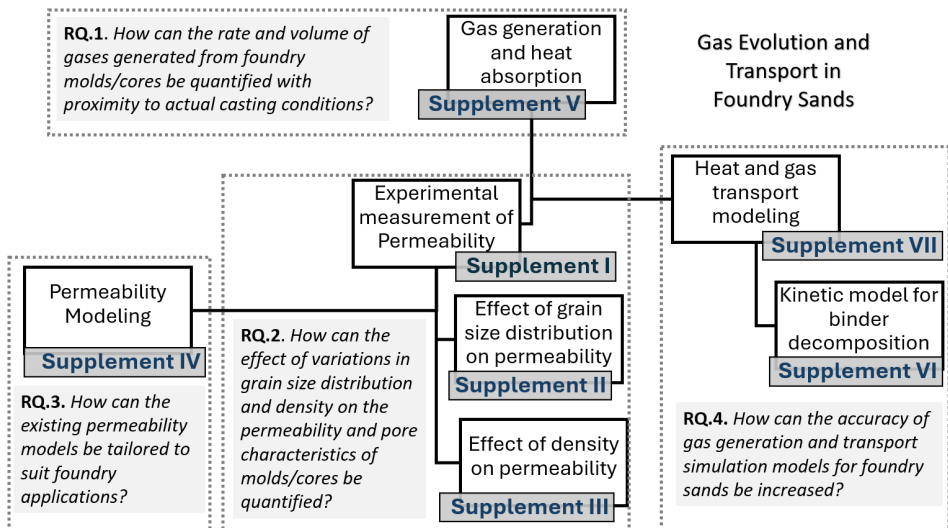


Figure 2.2 Overview of how the specific research questions are addressed using the supplements.

2.3 MATERIALS AND METHODS

This section discusses the materials investigated and the experimental methods designed and developed to quantify permeability and gas evolution. Also, the characterization techniques and analytical methods employed to analyze and study the samples are elaborated.

2.3.1 Materials

Foundry sand mixtures were prepared to study permeability and gas evolution. Baskarp sand, widely used in Sweden for foundry purposes, was the granular material/aggregate studied in this work. The binder system consisted of a self-setting furan-based (furfuryl alcohol-based resin) and sulphonic acid-based catalyst. For the furan samples, 2 % (of the weight of the sand) of resin was added. 40 % (of the weight of the resin) of liquid catalyst was added as the curing agent. The grain size distribution of the base sand measured using sieve analysis is shown in Figure 2.3. The sieve analysis was performed using a laboratory sieve shaker manufactured by Multiserw-Morek.

The sand consisted of multiple size fractions ranging from 0.063 to 1 mm. Also, from the results, it can be seen that the sand consists predominantly of 0.25 mm grains amounting to 57 wt. %. The average grain size calculated using multipliers according to Swedish standards was estimated to be 0.31 mm.

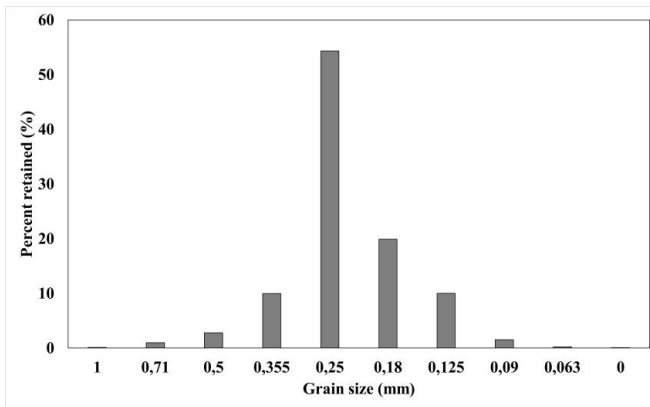


Figure 2.3 The sieve analysis results for the base sand used for preparing the samples investigated in this work.

Apart from the samples prepared using Baskarp sand and furan binder system, In the work reported in the supplement I, an additively manufactured sample prepared using cerabeads (mullite) with a rounded grain shape and uniform grain size was investigated. The samples were prepared using Baskarp sand and bound using the Furan binder system in the rest of the supplements.

Sample preparation for permeability measurement

For the permeability measurement, standard cylindrical samples were prepared according to DIN standards with the dimensions of 50 × 50 mm. The binder levels were kept constant for all the prepared samples, and the curing time was twenty-four hours. Figure 2.4 shows the prepared samples used for permeability measurement.



Figure 2.4 The cylindrical samples prepared according to DIN standards for permeability measurement.

Two separate studies were performed with respect to permeability, and two sets of samples with varying properties were prepared.

Samples studied using the developed permeability setup in supplement I.

The first supplement presents the experimental setup developed to measure the permeability of Foundry samples. Two samples were studied for this supplement. The properties of the samples investigated are presented in Table 2.1.

Table 2.1 The samples that were studied in supplement I.

Sample	3D Printed	Furan
Aggregate	Cerabeads	Silica sand
Grain size distribution (mm)	Single grain size of 0,14	0,063-1
Resin	Phenolic (2 %)	Furan (2 %)
Apparent density (g/cm ³)	1,441	1,445

Samples with varying average grain size distribution studied in supplement II.

In supplement II, the effect of varying grain size distributions was studied. As shown in Table 2.2, the base sand contained 10 % of 0.125 mm grains. The percentage of 0.125 mm grains was altered to create variation in the average grain size values. Sand collected from different sieves was mixed according to the proportions presented in Table 2.2. The average grain size (calculated according to the Swedish standards using multipliers) varied for the batches, as shown in Table 2.2. Batch A, B, and C were prepared with 0, 10,

and 20 % of 0.125 mm grains, respectively, and the resulting average grain sizes were 0.33, 0.28, and 0.24 mm, respectively.

Table 2.2 The proportions of the different batches mixed to obtain variations in grain size distributions (Supplement II)

Sieve opening, mm	Amount of Fraction, %			
	Basic Sand	A	B	C
1.000	0.104	0.12	0.09	0.07
0.710	0.988	1.10	0.88	0.66
0.500	2.808	3.12	2.50	1.87
0.355	9.980	11.09	8.87	6.65
0.250	54.350	60.39	48.31	36.23
0.180	19.932	22.15	17.72	13.29
0.125	10.000	0.00	20.00	40.00
0.090	1.540	1.71	1.37	1.03
0.063	0.222	0.25	0.20	0.15
0 (PAN)	0.077	0.09	0.07	0.05

A sample from each of the prepared batches was mixed with the Furan binder system and hand-rammed. A rammer with a stopper ensured constant dimensions for the samples. However, due to the manual compaction, there was a very slight difference in the density values. The density values presented in Table 2.3 were calculated directly using the mass and volume of the sample. The results of accurate density measurements using porosimetry and image analysis are presented in the results section.

Table 2.3 The results of the samples prepared using the different batches prepared for permeability measurement (Supplement II).

Sample	Amount of 0.125 mm fraction (%)	Density (g/cm ³)	Average grain size (mm)	Binder system
A	0	1.454	0.33	Furan 2 %
B	20	1.459	0.28	Furan 2 %
C	40	1.478	0.24	Furan 2 %

Samples prepared with variations in the apparent density studied in supplement III

For the third supplement, the grain size distribution of the base sand was unaltered. A known amount of the aggregate mixture (with resin and catalyst) was input into a tube and rammer setup, with a stopper attached to produce samples with constant dimensions (standard 50 × 50 mm). By altering the input weight of the mixture for compaction, variation in the resulting apparent density of the cured sample was achieved. The variation in the density was created by varying the input weight into the ramming tube and the compaction force to create samples with the same dimensions. The dimensions and parameters of the measured samples are provided in Table 2.4.

Table 2.4. The properties of the samples that were prepared for studying the effect of variation in density (Supplement III).

Sample	Mass (g)	Volume, (cm ³)	Density (g/cm ³)	Average grain size(mm)	Binder system
A	135.12	99.73	1.39	0.31	Furan 2 %
B	149.62	99.83	1.51		Furan 2 %

Sample preparation for the thermal analysis and gas generation measurement

Spherical sand samples of 40 mm diameter were prepared for the gas evolution measurements. The spherical shape was chosen to create a geometrical domain where polar, spherical coordinates can be applied during the analysis of the results. The binder level was constant at 1.2 wt % (with respect to the sand) for all the samples prepared. For the curing, 40 wt.% (with respect to the resin) of acid catalyst was added. The grain size distribution was unaltered from the base sand (Figure 2.3). The aggregate, resin, and catalyst mixture was hand-rammed into core boxes. The curing time for the sample was 24 hours.

2.3.2 Experimental Setup

Two experimental setups were developed as part of the work. The first setup was to quantify the permeability in standard measurement units. The second experimental setup was developed to quantify the volume of gases generated from molds/cores. In addition to the gas evolution measurement, simultaneous temperature curves for the molds and cores were measured.

Permeability

To measure permeability in standard units (m²), an experimental technique that is based on the Darcy law, which is prevalent in the field of earth sciences, was developed [18]. A brief description of the experimental setup is provided below.

The experimental setup (Figure 2.5) consists of a sample holder to hold the sand core, airflow tubes, differential pressure sensors, airflow meter, and data acquisition system. The sample was wrapped using a plastic heat shrink tube that provides an air-tight enclosure of the sand core. The tube and the sample were then covered using closing lids on both sides. Compressed air was passed through flow tubes, and the pressure was controlled using pressure regulators. A flow valve was employed to control the airflow rate. A differential pressure sensor was attached to measure the pressure between the input and output sides of the sample. The pressure sensor had an operating range of 0–2 kPa. The flow rate at the outlet end was measured using a flow sensor, which measured airflow ranges from 0–1 m/s. It is capable of detecting low flow rates. The volumetric airflow rate was obtained from the velocity measurements. The pressure was altered using the regulator during each measurement so that there was an increase in the flow rate. After each flow increase, there was a change in the differential pressure between the upstream and the downstream ends. The mass flow sensor in the downstream end measured the flow velocity for each inlet flow rate increase.

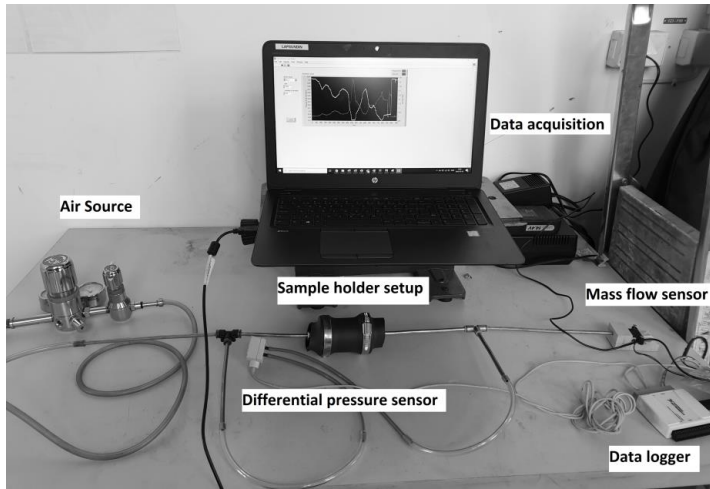


Figure 2.5 The experimental setup developed to measure permeability in standard units.

Thermal analysis and gas generation

The experimental setup developed for performing the thermal analysis and measuring the generated gas volume, termed Thermal analysis and gas generation (TAGG), is elaborated in this section. The TAGG setup includes special sample preparation steps before the actual experiment. These steps enable simultaneous temperature and gas evolution measurements for foundry molds and cores. The \varnothing 40 mm spherical samples were drilled to incorporate thermocouples and quartz tubes at the exact locations shown in Figure 2.6 [105].

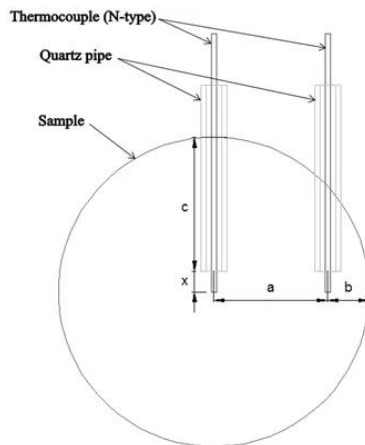


Figure 2.6 The sample setup for the TAGG measurements [105]. The dimensions of the different variables are provided in Table 2.5.

Table 2.5 The dimensions of the different variables.

Diameter of the specimen (mm)	Dimensions (mm)			
	a	b	c	x
40	10	10	15	5

Thermocouples (TC) help provide the heating curve data in the central (TC1) and lateral (TC2) parts of the sample. The quartz tubes serve two purposes: they protect the thermocouples from the melt, and the central quartz tube also acts as the evacuation route for the evolving gases to be collected. The connection between the sample, quartz tubes, and the holder was made using a ceramic adhesive composed of silica powder capable of withstanding temperatures up to 1370°C.

The experimental setup of the TAGG measurement, which includes several components, is shown in Figure 2.7. The molding material sample (a), Figure 2.7, is immersed into the molten metal (b). The diameter of the quartz tube protecting TC1 has $\varnothing_{\text{outer}} = 9$ mm, $\varnothing_{\text{inner}} = 7$ mm whereas, the tube protecting TC2 has $\varnothing_{\text{outer}} = 5$ mm, $\varnothing_{\text{inner}} = 3$ mm. It is sealed with a heat-resistant powder to ensure the gas evacuation from the sample happens exclusively through the central tube, protecting TC1. The thermocouples and protecting pipes are mounted in the sample holding unit (c). The thermocouples, quartz tubes, and the molding material sample are held together with a specially designed holder mechanically, including small plates and screws. Furthermore, the central tube is connected to a horizontal quartz pipe ($\varnothing_{\text{outer}} = 7$ mm, $\varnothing_{\text{inner}} = 5$ mm, (d), which in turn connects the sample unit to a resistance-heated pipeline (e). The role of the pipeline heating unit is to avoid temperature decrease of the evacuating gases and consequent gas condensation, also reported in the literature. The collected gases are transported through the heated pipeline (170 °C) into a liquid displacement beaker (f) containing preheated Rapeseed oil. The oil is preheated to 140 °C before the sand sample is immersed into the molten liquid to avoid changes in the oil's viscosity and maintain a stable flowability between the liquid displacement beaker and the oil sampling beaker placed on a digital scale. The mass of the displaced oil is measured using a precision balance with a logging frequency of 5 readings per second (g). Each sample measured is immersed in the melt for approximately 300 seconds. The samples measured were at room temperature during the immersion process. Signals from the thermocouples and the digital balance are collected in a data acquisition device with five readings per second logging frequency. The volume of gases evolved is calculated using the known density values of the oil. Since the maintained oil temperature during the measurement was close to 140 °C, a constant value of density 0.85 g/cm³ was used to calculate the volume of the gases evolved [106].

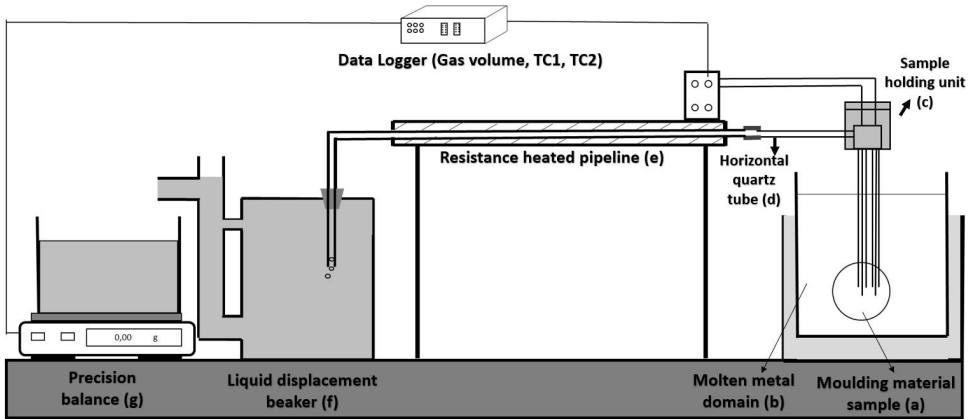


Figure 2.7 Schematic illustration of the thermal analysis and gas generation (TAGG) instrument.

2.3.3 Material characterization

Mercury intrusion porosimetry

Mercury intrusion porosimetry involves intruding mercury, which is a non-wetting liquid, into the porous material [76]. The pressure required to intrude the non-wetting liquid into the material is inversely proportional to the pore size. Mercury is the most widely used non-wetting liquid in this category. The relationship between the pore size and the pressure is given by the Washburn equation (Equation 14).

$$P = \frac{-2\gamma \cos \theta}{r}$$

Equation 14

where P is the pressure (MPa), γ is the surface tension (interfacial energy) of the mercury (N/m) and θ is the contact angle of mercury with the material (deg) [76].

The sample preparation requires some care because the sample holder has size restrictions, and for chemically bonded sands, a sample of the required size needs to be carved/cut out of bigger cores or small cores that are within the size requirements should be prepared.

The samples preserved after the permeability measurement were cut and prepared for the Mercury intrusion porosimetry study. The dimension of the samples investigated was $14 \times 14 \times 14$ mm. As a requirement for the MIP, the samples were dried in a furnace for 24 hours to eradicate the free moisture.

Mercury intrusion porosimetry (MIP) was performed using Micro metrics Autopore III 9410 equipment at the research institute, RISE, Sweden. The surface tension and contact angle of mercury were set to 485 mN/m and 130° , respectively. For the porosimetry measurements, three positions from each sample were identified and cut from the cylindrical furan sand sample (Figure 2.8).

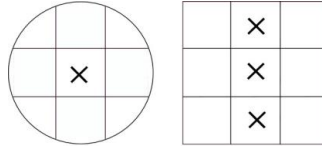


Figure 2.8 The sample position cut from the cylindrical samples for the mercury porosimetry measurement.

X-Ray microtomography

The main working principle behind the technique is the relationship between x-ray absorption and material density. The method can be considered an upgrade to the CAT (computerized axial tomography) scan technique, which has its roots in projection radiography used in the medical imaging field [107]. The method works based on two underlying principles: X-ray absorption and tomographic reconstruction mathematics. An illustration of the working principle behind this method is shown in Figure 2.9. Images in the form of 2D slices can be obtained from X-ray microtomography (X-ray μ CT), and such images are processed and analyzed to study and quantify materials.

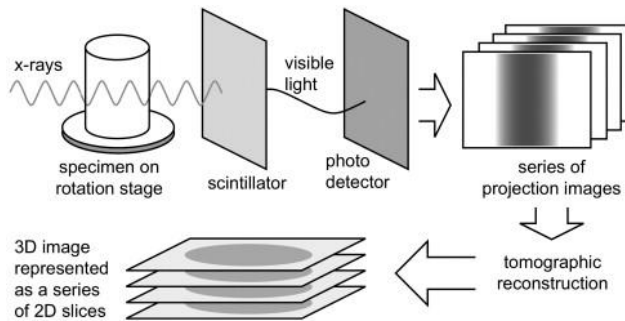


Figure 2.9 The schematic illustration of the X-ray microtomography technique

The sections of the sample preserved after permeability measurement (Figure 2.10) were prepared for the tomography measurement. The dimension of the samples investigated was 14×14×14 mm.

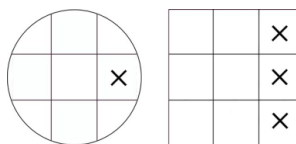


Figure 2.10 The sample position cut from the cylindrical samples for the X-ray microtomography measurement.

The obtained images provided an opportunity to determine the size and shape of the grains accurately. Circularity was measured based on the standard definition used in

particulology [30]. The image slices obtained from the x-ray microtomography were processed and analyzed using the open-source image processing tool Fiji (ImageJ) [108].

Thermogravimetry

For the thermogravimetry measurement, Furfuryl alcohol-based resin was polymerized using an acid catalyst consisting of Benzene sulphonic acid (35–50 wt.%), Xylene sulphonic acid (25–35 wt.%), Methanol (3–10 wt.%), and Toluene sulphonic acid (<10 wt.%). Small pieces of the polymerized Furan were evaluated to study the kinetic parameters (Approximately 100 mg of the Furan sample was placed in the crucible). TG analysis and DTA were performed for the furan sample to investigate the decomposition rate of the furan during the heating process. The study was conducted using the TG-DTA apparatus (Derivatograph C/PC, MOM Szeviz Kft.). The temperature was increased from 298 K to 1173 K with three different heating rates: 2 K/min, 7 K/min, and 17 K/min in the air atmosphere. The weight changes of the sample and the DTA signals were recorded on the computer against time and temperature.

2.3.4 Modeling the heat and gas transport in sand core/mold

The heat and gas transport modeling was implemented using COMSOL Multiphysics. The model structure and coupling between the physics domains are shown in Figure 2.11.

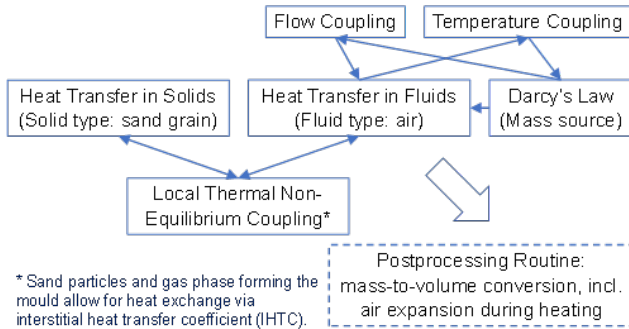


Figure 2.11 The simulation model structure

A local thermal non-equilibrium condition was assumed to account for the heat transfer between the sand and the fluid domain in the porous material. The gas flow was approximated with Darcy's flow, and the mass source term was incorporated into the continuity equation.

A symmetrical spherical model was developed, including the aperture for gas evacuation, such that the TAGG experiment can be used to validate the developed heat and gas transport model. In the post-processing routine, a mass-to-volume conversion was performed to compute the volume of the gases generated. The thermophysical properties of the mold and core were not measured, and instead, thermal conductivity and specific heat capacity as a function of temperature were adopted and calibrated (to fit temperature curves) from material databases of commercially available simulation tools [101].

CHAPTER 3

SUMMARY OF RESULTS AND DISCUSSION

CHAPTER INTRODUCTION

This chapter summarizes the main results of the performed work and the appended supplements.

3.1 GAS TRANSPORT

3.1.1 Permeability

The results of the permeability measurement are presented in the upcoming sections. An overview of the work related to the permeability of foundry molds and cores is provided in Figure 3.1.

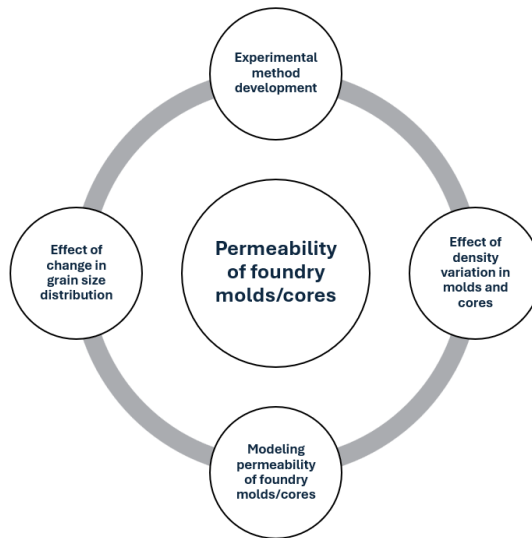


Figure 3.1. An overview of the work performed related to permeability

Method development (supplement I)

Two approaches were adopted with the developed experimental setup. The first was a steady-state approach where the pressure and flow velocity data were obtained only after the sample reached a constant pressure and velocity. In the second type of measurement, no time for saturation was given. In this unsteady type of measurement, the increase in the flow rate and the corresponding increase in the flow rate are analyzed.

The Δp vs. flow rate curve indicates a linear relationship, so airflow could be considered as in the case of an incompressible fluid [109]. Using the raw-data curves, the ratio between the volumetric flow rate, Q , and the cross-sectional area of the measured sample, A , is plotted against the ratio between the differential pressure, Δp , and the length of the sample, L . Permeability was computed from data obtained from both the approaches.

Since the measured flow rates were low, inertial effects were ignored, and the Forchheimers equation was not used for the computation; instead, the Darcy equation was used to compute the permeability (Equation 15).

$$Q = \frac{K \cdot A \cdot \nabla p}{\mu \cdot L}$$

Equation 15

Using the data from the experimental setup, a plot between the volumetric flow rate of the air through the outlet side of the sample, Q , divided by the cross-sectional area, A , of the sample was plotted against the ratio between the differential pressure, ∇p , and length of the sample, L . The Q/A as a function of $\nabla p/L$ for the samples with varying grain size distribution is shown in Figure 3.2 (unsteady-state approach). The slope of these plots provides the value of k/μ , where k is the permeability and μ is the viscosity of the fluid passing through the porous material.

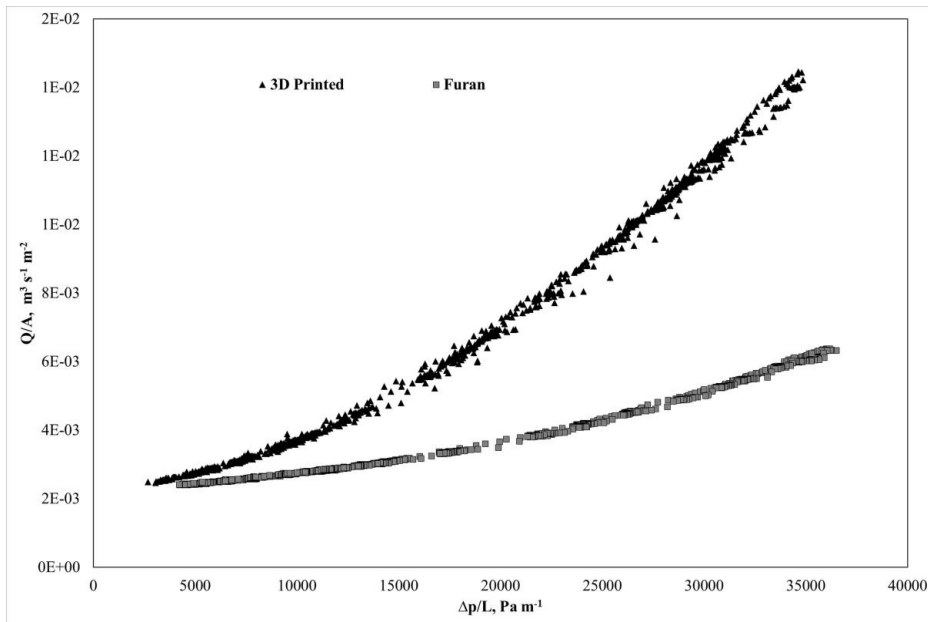


Figure 3.2 The Q/A plotted as a function of $\nabla p/L$ for the samples measured.

Since compressed air was used as the fluid during measurements, the dynamic viscosity of air obtained from the literature [18] was used to compute the permeability of the measured samples. The results of the permeability measured for the two samples investigated are presented in Table 3.1.

Table 3.1 The results of the steady-state and the un-steady state type of measurements

Sample	Permeability (m ²)		Standard deviation	
	Steady-state	Unsteady-state	Steady-state	Un-steady-state
Furan	1.95E-12	2.13E-12	±0.063	±0.062
3D-Printed	7.05E-12	7.04E-12	±0.19	±0.20

Effect of variation of grain size distribution (Supplement II)

The results of the permeability measurement for samples with varying grain size distribution are elaborated in Supplement II. The results of the Q/A and dP/L are shown in Figure 3.3. The permeability results for samples with varying grain size distribution are presented in Table 3.2.

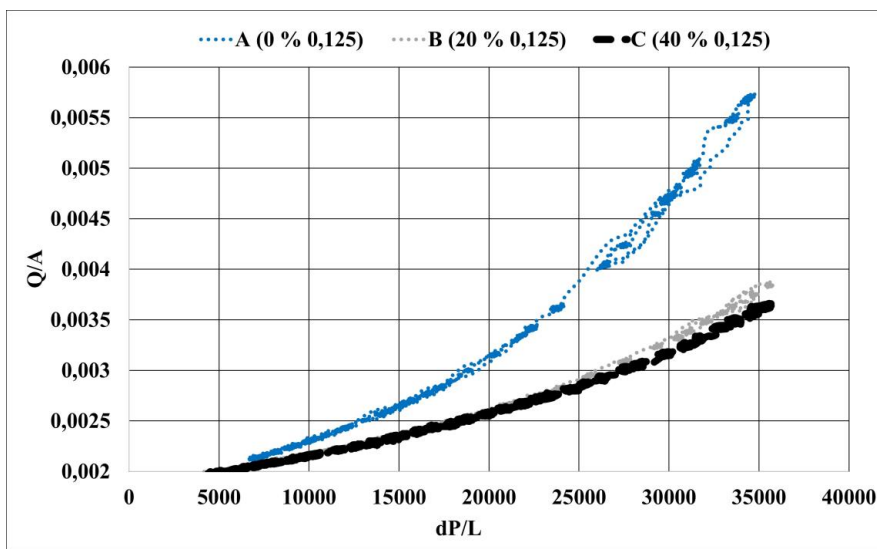


Figure 3.3. Experimentally obtained plot of Q/A as a function of dP/L , from which the permeability is computed for samples with varying grain size distributions.

Table 3.2 Permeability results for the samples with varying grain size distributions.

Nomenclature in the supplement	Average grain size distribution (mm)	0,125 mm grains (%)	Apparent density (g/cm ³)	Binder level (%)	Binder System	Permeability (m ²)
A	0.33	0	1.45	2	Furan	2.05E-12
B	0.28	20	1.45	2	Furan	1.04E-12
C	0.24	40	1.47	2	Furan	9.56E-13

The permeability decreases with the average grain size, as expected. However, the difference between samples B and C is not very significant. The results are discussed in connection with the mercury porosimetry measurement results.

Effect of variation of the density of cores (Supplement III)

The Q/A vs. dP/L plot for the samples with varying densities is shown in Figure 3.4. The permeability results for samples with varying grain size distribution are presented in Table 3.3.

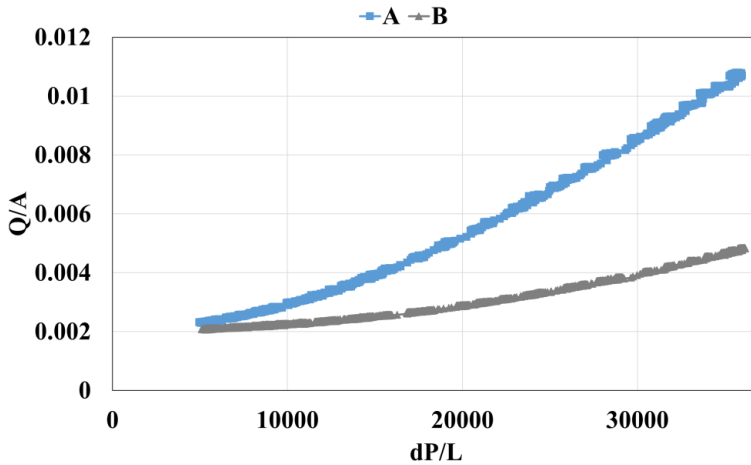


Figure 3.4 The Q/A vs. dP/L plot for samples with varying density

Table 3.3 The results of the permeability of samples with varying apparent density.

Nomenclature in the Supplement	Average grain size distribution (mm)	Apparent density (g/cm ³)	Binder level (%)	Binder System	Permeability (m ²)
A	0.31	1.39	2	Furan	5.26E-12 ± 0.09
B	0.31	1.51	2	Furan	1.43E-12 ± 0.18

The results show the expected trend where an increase in apparent density resulted in decreased permeability. The steeper the slope of the Q/A as a function of dP/L, the higher the permeability of the sample.

3.1.2 Pore structure characterization

Mercury intrusion porosimetry

The porosity and pore characteristics analysis was performed for the samples with varying grain size distributions and samples with varying density to find how these parameters influenced the permeability of the cores.

Variation in grain size distribution (Supplement II)

Three positions from each sample were studied to determine how compaction can result in localized variations of porosity, pore size distributions, and apparent density. The results show localized variation for the three positions within the same sample. There is approximately a 1-3 % difference in the porosity within the same sample and a 1-4 μm difference in the median pore diameter between the different positions of the same sample. These differences affect the permeability and the localized venting ability of foundry cores in different regions.

Sample A, with 0% 0.125 fractions, had a higher concentration of the larger pores (250–130 μm) and a lower concentration of smaller pores (130–75 μm). Sample B, when compared with A, showed a slightly lower number of pores for both categories. However, sample C showed a different trend where the larger pores were lower in concentration, and the smaller pores were higher in concentration. The summary of the pore characteristics is provided in Table 3.4.

The results show that the median pore diameter decreases for the sample with a lower average grain size. The porosity, however, is seen to increase for the sample with the lowest average grain size. This is contrary to what is expected. This is because sample C has a significantly higher amount of smaller pores and a higher total porosity. It also has the lowest median pore diameter. This is not the case with samples A and B, where the pore diameter was higher while these samples exhibited slightly lower porosities. The pore diameter is vital and influences the permeability because the pore diameter affects the velocity of the fluid passing through the sample and the differential pressure between the inlet and the outlet side of the sample.

The results indicate that porosity is not directly proportional to the permeability. The pore characteristics (like in Sample C, where there is a large amount of relatively smaller pores) dictate the material's permeability.

Table 3.4. The results of the porosimetry and the pore characteristics for samples with differing grain size distributions.

Property	Sample		
	A	B	C
Pore volume (cm^3/g)	0.287	0.287	0.300
Median pore diameter (μm)	71.33	69.33	65.33
porosity (%)	42.66	43.00	44.33
Bulk density (g/cm^3)	1.495	1.494	1.488
True density (g/cm^3)	2.602	2.631	2.684
Percent intrusion at d_{crit} (%)	86.25	80.87	72.07
d_{crit} (μm)	72.66	72.49	72.64

Variation in density (Supplement III)

The results of mercury porosimetry for the samples with varying densities showed that the critical pore diameter can vary with significant differences in the apparent density. Also, the pore network varies significantly, too. Sample B had a lower volume of larger

pores of 230–130 μm . On the other hand, Sample A had a higher volume of larger pores and a lower volume of smaller pores, both in the range of 130–80 μm and 0.1–0.009 μm . Sample B had a lower porosity, relatively fewer macropores, and a lower critical pore diameter. It is, however, interesting to see the significantly higher number of meso-micro pores in Sample B.

X-Ray micro-tomography (Supplement IV)

The pore characterization of the experimentally investigated samples was also subjected to X-ray microtomography characterization. All five samples, three with varying grain size distribution and two samples with varying apparent densities, were characterized. The porosity and pore size distribution obtained from X-ray microtomography are compared with the mercury porosimetry data. Other critical parameters, such as tortuosity, grain shape, and size parameters that cannot be quantified using other methods, were also determined using the tomography results.

Grain parameters

The estimated grain size distribution and grain diameter from x-ray microtomography and image analysis tools are presented in Table 3.5. The percentile value providing the most significant difference was the median grain diameter, D_{mg} , and it was identified as the effective diameter. The average grain diameter measured from image analysis shows that the mean value is much smaller than the traditional average grain size calculation done using sieve analysis and multipliers.

Table 3.5. Circularity and average grain diameter computed with image analysis (IA) and sieve analysis (SA)

Sample	Grain diameter (μm)			Circularity
	Median D_{mg}	Mean, (IA)	Mean, (SA)	
A	233	247	330	0.79
B	220	238	280	0.78
C	208	228	240	0.78
D	236	251	310	0.79
E	225	240	310	0.78

Pore characteristics

The porosity, pore diameter, and tortuosity of the samples were measured from images obtained using X-ray micro-tomography. The results (including results from mercury porosimetry) are presented in Table 3.6.

Table 3.6 The pore characteristics of the different samples measured using image analysis (IA) and mercury porosimetry (MP)

Sample	ϕ (IA)	ϕ (MP)	$D_h, \mu\text{m}$	$D_{mp}, \mu\text{m}$		T	$h, \mu\text{m}$
			Mean	(IA)	(MP)	Mean	Median
A	0.45	0.43	145	106	71	1.025	128.0
B	0.45	0.43	143	100	69	1.238	125.3
C	0.44	0.45	126	87	65	1.245	118.0
D	0.48	0.48	164	129	101	1.027	140.8
E	0.43	0.43	127	99	69	1.238	128.6

Permeability prediction models

Pore space models to predict permeability use the term specific surface area or specific internal volume of pores. However, some grain size-based models, like the Kozeny-Carman equation, use the specific surface area of grains. The original Kozeny theory model refers to the specific surface area of the porous channels. In the literature, this distinction has not been addressed clearly and some researchers have erroneously used them interchangeably.

The most suitable prediction model was identified by comparing the experimentally obtained and computed permeability values.

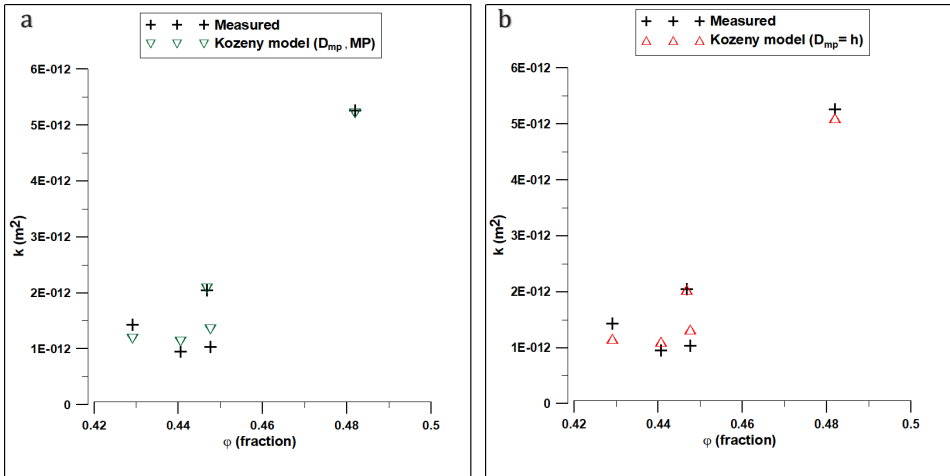


Figure 3.5. The predicted and experimental permeability values plotted against the porosity of the investigated samples. Median pore diameter by mercury porosimetry (a), Median pore diameter by mercury porosimetry (neglecting the pore height) (b)

The evaluation results of different models show that the original Kozeny model is the most suitable for foundry molds and cores. Figure 3.5 shows the predicted permeability using the median pore diameter obtained from mercury porosimetry.

Modification of the original Kozeny theory model

For materials such as sandstones, modifications have been done to predict permeability using simple terms [83]. Understanding the process parameters is essential to create such a modification for foundry cores and molds. Since grain size distribution and compaction determine the pore space for foundry molds and cores, compaction was quantified using the porosity of molds/cores. A factor to estimate the effect of compaction, termed compaction factor, f_c , has been elaborated in supplement IV.

The OKT model, when assuming the median pore diameter and height of the cylindrical pore are equal (neglecting the need to measure the pore height), can be rewritten as Equation 16, by incorporating the term $(6/D_{mp})^2$ for specific internal volume.

$$k = \frac{c\varphi^3}{36} \cdot \frac{D_{mp}^2}{T^2}$$

Equation 16

By establishing a relationship between the effect of compaction, porosity, and grain diameter with the median pore diameter and tortuosity ratio, a modified version of the OKT model was established (Equation 17).

$$k = \frac{c\varphi^3(4 \cdot 10^5 k_0^{2.51})^2}{36}$$

Equation 17

where $c = 0.17$ for the studied foundry samples. The permeability values obtained from the modified version of the Kozeny model compared with the experimentally obtained permeability are presented in Table 3.7. The results show that the new model that uses easy-to-obtain parameters can predict permeability accurately.

Table 3.7 The results of the estimated and experimental permeability

Sample	Permeability (m ²)	
	Modified OKT model	Measured
A	2.11×10 ⁻¹²	2.05×10 ⁻¹²
B	1.61×10 ⁻¹²	1.04×10 ⁻¹²
C	1.03×10 ⁻¹²	9.56×10 ⁻¹³
D	5.00×10 ⁻¹²	5.26×10 ⁻¹²
E	1.16×10 ⁻¹²	1.43×10 ⁻¹²

3.2 GAS GENERATION (Supplement V)

3.2.1 Raw data of gas generation and temperature

Three samples (A, B, C) produced from the same batch of sand mixture were immersed in the liquid cast iron melt using the TAGG setup. The properties of the investigated samples are provided in Table 3.8.

Table 3.8 Weight, volume, the apparent density of sand samples, and generated gas volume.

Sample	Weight (g)	Volume (cm ³)	Apparent density (g/cm ³)	Generated gas volume (cm ³)
A	53.4	33.5	1.59	1060
B	53.5		1.59	1115
C	53.3		1.59	1129

The variation of the sample weight and apparent density was negligible, which resulted in similar heating curves. The difference in gas volume measured could be due to several possible reasons. Variation of the local density values along the spherical samples could be caused by the hand ramming process applied during the production of the samples. In addition, the local inhomogeneity of the granular interspace may have caused regional variation in access to oxidizing elements, which may delimit the binder decomposition by combustion, instead promoting decomposition by pyrolysis [110].

3.2.2 Thermal analysis

Fourier thermal analysis (FTA) is an applied analysis method initially developed for the calculation of the released latent heat of solidification based on analyses of the temperature differences registered in the solidifying cast alloy [111]. The authors developed an extension of the FTA method [112] for calculating the heat absorption during the decomposition of the organic binders in sand cores/molds. The heat absorbed is given by Equation 18.

$$q_{\text{abs}} = c_V \alpha \nabla^2 T - c_V \dot{T}$$

Equation 18

where q_{abs} is the rate of heat absorbed; c_V is the volumetric heat capacity; α , the thermal diffusivity; $\nabla^2 T$ is the Laplace operator characterizing the temperature differences in the domain and \dot{T} represents the local heating rate.

Equation 18 can also be written as,

$$q_{\text{abs}} = c_V(t)(Z_f(t) - \dot{T}(t))$$

Equation 19

where,

$$Z_f(t) = \alpha(t) \nabla^2 T(t)$$

Here, the $Z_f(t)$ is termed as the zero line, which represents the case when there is an absence of a heat-absorbing process (i.e., lacking binder decomposition). The calculated zero line Z_F , and the registered heating rate \dot{T} in the central thermocouple (TC1) of an experimental measurement (Sample C) is shown in Figure 3.6.

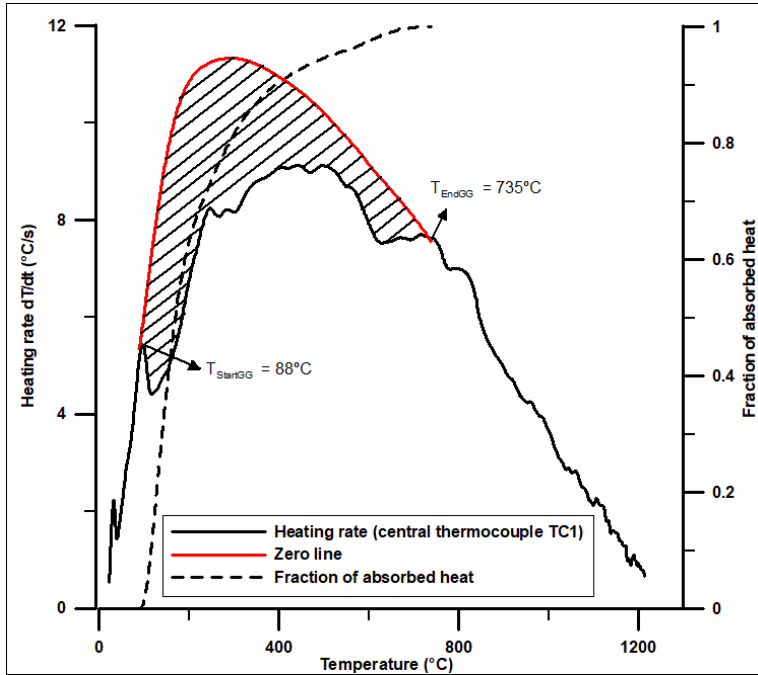


Figure 3.6 The results of the heat absorption calculation performed using FTA method. The difference between the heating rate, when there is an absence of binder (in a hypothetical case) and the actual heating rate (when there is binder), is shown in the shaded area.

Figure 3.6 also contains a cumulative curve (represented by the dotted lines) of the calculated absorbed heat during the gas generation process, f_a . The shaded area shows how, in the presence of binder, the heating rate is reduced, indicating heat absorption due to the decomposition process from the solidifying melt during the casting. In the figure, the surface area between the registered heating rate and the calculated zero curve is proportional to the time-dependent heat absorption (q_{abs}).

The gas generation interval starts at $T_{StartGG} = 88\text{ °C}$ and ends at $T_{EndGG} = 735\text{ °C}$. The volumetric heat capacity at the beginning $c_{V_StartGG} = 12.24\text{ MJ}\cdot\text{m}^{-3}\cdot\text{K}^{-1}$ and at the end of the gas generation interval $c_{V_EndGG} = 16.3\text{ MJ}\cdot\text{m}^{-3}\cdot\text{K}^{-1}$ are obtained from the literature[101]. Integrating the absorbed heat over the gas generation process between t_b and t_e , the total absorbed heat L was found to be equal to $650\text{ kJ}\cdot\text{kg}^{-1}$. Where, t_b represents the start of the decomposition process and t_e refers to the end of the decomposition process.

3.2.3 Gas generation kinetics

Figure 3.7 shows the results of the gas generation kinetics analysis combined with the thermal analysis. The peak of the released gas at the beginning is due to the expansion of the intergranular gaseous environment and the instant vaporization of the moisture in

the sample, driven by the rapid heating of the outer sand mixture layer. Gas generation in the outer domain ends at $t = 65$ seconds, when $T_{\text{EndGG}} = 735$ °C is measured on TC2. Gas generation in the inner domain of the sample starts at $t = 23$ seconds, when at the outer thermocouple, the temperature was $T_{\text{StartGG}} = 88$ °C. The gas generation completed at $t = 114$ s, when $T_{\text{EndGG}} = 735$ °C was measured on the inner thermocouple.

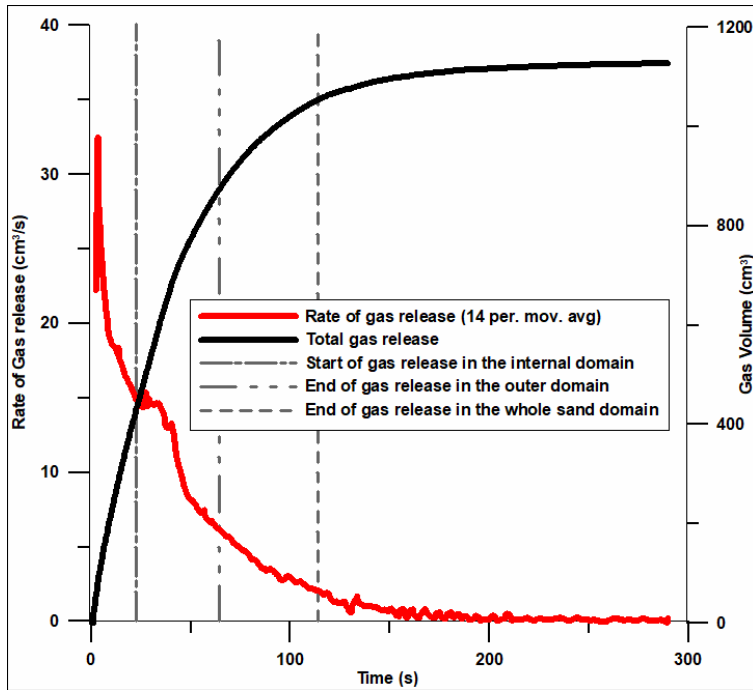


Figure 3.7 The rate of gas generation combined with the thermal analysis results.

3.3 MODELING OF HEAT AND GAS TRANSPORT

3.3.1 Kinetic model for binder decomposition (Supplement VI)

The thermogravimetry results with different heating rates were used to compute the kinetic parameters by assuming several single order apparent reactions. Using the integral method [113], the kinetic parameters of the decomposition of Furan resin were computed. A novel approach of utilizing a series of assumed apparent single-order reactions enabled the computation of the kinetic parameters for the complex foundry binder decomposition process.

The linear regression analysis performed to determine the kinetic parameters is presented in Figure 3.8. The parameters for the five apparent reactions were computed using the obtained thermogravimetry data.

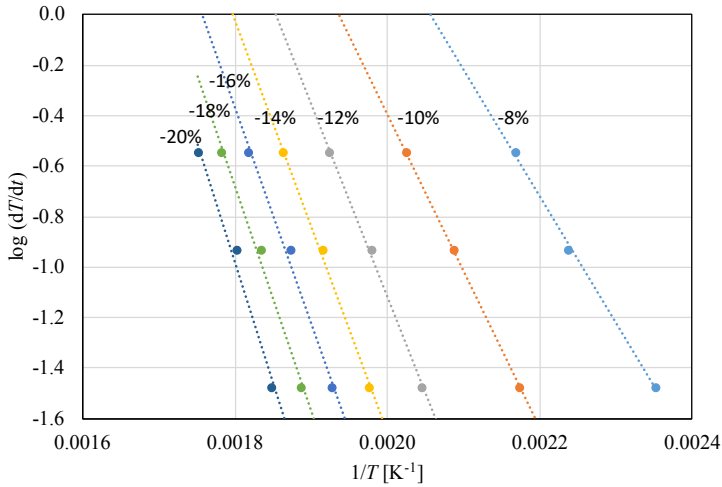


Figure 3.8 The linear regression analysis performed to determine the activation energy and the pre/exponential factor using the TG data.

The activation energy and the pre-exponential factor for the different reactions are presented in Table 3.9. The table also provides information about the reaction trigger temperature or onset temperature. It has to be noted that during the actual casting process, due to the extremely high heating rates, the trigger temperatures should be slightly higher than what is estimated using TG, where the conditions are close to equilibrium.

Table 3.9 Activation energy Q and the pre-exponent factor A for each reaction (each TG range) and corresponding temperatures.

Apparent reaction	Weight loss (TG range)	Corresponding temperature [K]	A (s^{-1})	Q ($J \cdot mol^{-1}$)
1	From 0 to -8%	R.T. - 424	1.101×10^7	7.424×10^4
2	From -8 to -20%	424 - 542	1.234×10^{13}	1.406×10^5
3	From -20 to -35%	542 - 653	4.750×10^{20}	1.882×10^5
4	From -35 to -60%	653 - 778	26.29	5.568×10^4
5	From -60 to -100%	778 - Max.	7.726×10^{-2}	4293

Using the multi-reaction model, the different kinetic parameters were obtained, and the pressure build-up in the core was estimated. For this purpose, a simplified core geometry was created. The results show that the pressure predicted using the multi-reaction approach is much higher than the single-reaction approach that the commercial tools employ (Figure 3.9).

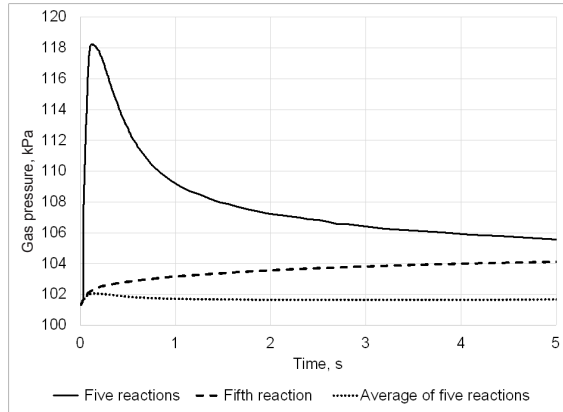


Figure 3.9 The predicted pressure for the simplified core geometry estimated using the five-reaction approach compared with the usage of a single average value of the activation energy.

3.3.2 Computational modeling of heat and gas transport in sand mold/core (Supplement VII)

In order to accurately simulate the heat and mass transport in foundry sand cores, a computational model that incorporates the experimentally measured permeability, gas generation data, and kinetic model was developed. A local thermal non-equilibrium situation in the porous sand core was modeled by coupling the heat equations for solid and liquid phases to describe the heat transfer. The experimentally obtained permeability and porosity were employed in combination with Darcy’s law to compute the flow properties. The developed kinetic model, including the five apparent reactions for the binder decomposition, formulated the gas source.

Dried Furan samples were measured for gas evolution and heating curves using the developed TAGG setup. The experimentally obtained gas volume was used to validate the developed computational model.

A comparison between the measured and the simulated heating curves shows good agreement (Figure 3.10).

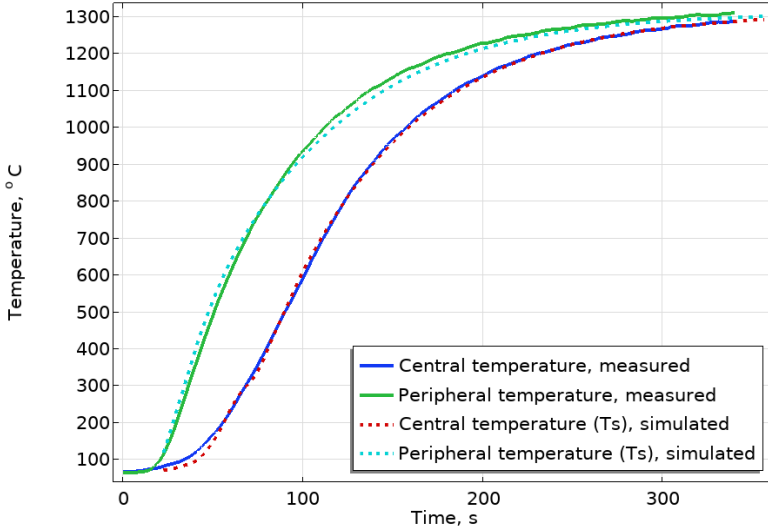


Figure 3.10 The measured and the simulated temperatures at locations of the central and the peripheral thermocouples.

The mass-to-volume conversion was performed, considering the volume of gases generated due to the decomposing binder and the already present air that expanded during the thermal shock. The results of the simulated gas volume plotted against time in comparison to the experimentally obtained values are shown in Figure 3.11. Although these are initial validation results, a certain level of validity of the computational model has been confirmed.

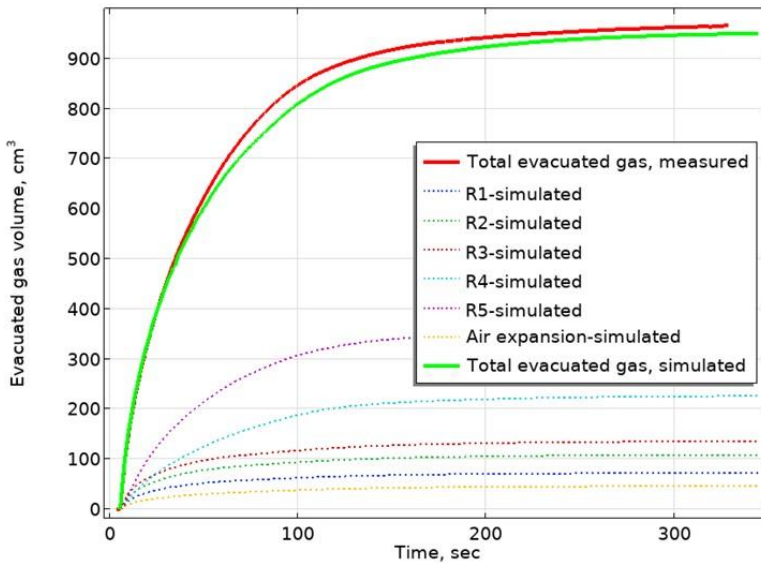


Figure 3.11 The measured and simulated gas volume results for the studied sample.

CHAPTER 4

CONCLUSIONS

The main conclusions of the thesis work are provided in this section. The findings pertaining to each research question have been addressed individually.

RQ.1. *How can the rate and amount of gases generated from foundry molds/cores be quantified with proximity to actual casting conditions.?*

A novel thermal analysis and gas generation method (TAGG) has been developed to quantify the volume of gases generated from different molding mixtures. The experimental conditions of the developed method replicate the conditions an actual core/mold is subjected to during the sand-casting process. The developed method includes the measurement of temperature profiles of the molding material sample, providing the opportunity to perform robust thermal analysis measurements.

The method provides the rate of gas generation and volume of gases generated as a function of time. It gives the possibility to compute the effect of decomposing binders and the generated gases on heat absorption.

RQ.2. *How can the effect of variations in grain size distribution and density on the permeability and pore characteristics of molds/cores be quantified.?*

An experimental method to determine permeability in standard units of m^2 was developed, and samples with varying grain size distribution and density were measured. The results show that the pore diameter influences the permeability of samples with similar porosities. The critical pore diameter does not vary for samples with varying grain size distribution, creating lesser (but significant) differences in permeability. The pore characterization also shows that most pores in a foundry sample fall within a 130-50 μm range.

On the other hand, samples with varying densities show that the critical pore diameter could vary, creating significant differences in permeability. The increase in density significantly affects the median pore diameter of the molds and cores.

RQ.3. *How can the existing permeability models be tailored to suit foundry applications?*

Most available models in the literature were tested to find the most suitable model to predict permeability. The results show that the original Kozeny model predicts the permeability of foundry molds and cores accurately and better than the most commonly used Kozeny-Carman model. The identified original Kozeny model is pore-space based, which also incorporates the opportunity to include the effects of production parameters such as compaction.

Although the model predicts permeability well, the parameters needed to perform prediction are complex and not easy to obtain. To tackle this, a relationship between the complex parameters, such as median pore diameter and the tortuosity, is established, and

using this relationship, the original Kozeny model is modified to suit foundry application. The resulting model can predict the permeability of foundry cores and molds using porosity and grain diameter. The model also can predict permeability in localized regions.

RQ.4. *How can the accuracy of gas generation and transport simulation models for foundry sands be increased?*

A local thermal non-equilibrium finite element model for heat and mass transport in a Furan resin sand core was developed. The developed methodology can be applied to other types of foundry sands. The numerical model can accurately predict the gas velocity and volume, gas temperature, and pressure at local regions of the core. The experimental gas volume and temperature distribution from TAGG measurement provided the opportunity to validate the developed numerical model. Although the results are presented for simple geometry, the model can be extrapolated to simulate advanced industrial castings.

Additionally, the simulation results show qualitatively that the prediction of pressure build-up in the cores using existing tools with a single reaction model for the binder decomposition results in underestimation.

FUTURE WORK

The work has opened up the possibility of exploring additional aspects related to gas evolution, defect formation, and property prediction of cast components.

Permeability of foundry cores and molds

The effect of expanding sand grains and the decomposing binder on the porosity and permeability must be studied.

Mold/core coatings influence the surface properties of the cast component. Several different types of coatings exist, and the components involved in the production of coatings vary depending on several factors, such as cost, production, and application. Although it is clear that the coatings increase the pressure build-up in the cores, the effect of coatings on the gas evolution, pressure build-up, and the permeability of cores needs to be studied.

Heat absorption and its effect on the properties of a cast component

The heat absorption calculations resulting from the binder decomposition and gas evolution vary with varying binder material. The influence of the reactions involved during the decomposition of the binder material can result in different rates of heat absorption at various points in time during the solidification process. The influence of this on the cooling rate of the cast component has remained an unexplored area of research.

Thermophysical properties of the mold/core

The thermophysical properties of the mold and core, such as the temperature-dependent thermal conductivity, are not accurately available today due to the difficulty in determining these parameters for complex granular systems such as sand molds. However, accurately determining the thermophysical properties helps researchers and foundries simulate the sand-casting process better, enabling better defect and property prediction.

Characterization of the gases generated from foundry molds and cores

Although a lot of work is being done on the environmental aspects of the gases generated from foundries, there are shortcomings in accurately determining the composition of the generated gases. The work in this direction focuses on quantifying the environmentally undesired gases. However, from the results of this work, it can be seen that the mass-to-volume conversion, which is a crucial step in estimating gas generation, requires accurate density measurement for the different binder systems used by foundries today.

REFERENCES

- [1] <https://www.caef.eu/statistics/>.
- [2] V. Biringuccio, *Pirotechnia*, MIT Press, (1966).
- [3] G.T. Kridli, P.A. Friedman, J.M. Boileau, *Manufacturing processes for light alloys*, LTD, 2020. <https://doi.org/10.1016/B978-0-12-818712-8.00007-0>.
- [4] R. Siddique, G. Singh, M. Singh, Recycle option for metallurgical by-product (Spent Foundry Sand) in green concrete for sustainable construction, *J. Clean. Prod.* 172 (2018) 1111–1120. <https://doi.org/10.1016/j.jclepro.2017.10.255>.
- [5] S. Fiore, M.C. Zanetti, Industrial treatment processes for recycling of green foundry sands, *Int. J. Cast Met. Res.* 21 (2008) 435–438. <https://doi.org/10.1179/136404608X373159>.
- [6] G. Gyarmati, I. Budavári, G. Fegyverneki, L. Varga, The effect of sand quality on the bending strength and thermal distortion of chemically bonded sand cores, *Heliyon* 7 (2021). <https://doi.org/10.1016/j.heliyon.2021.e07624>.
- [7] J. Sertucha, J. Lacaze, Casting Defects in Sand-Mold Cast Irons—An Illustrated Review with Emphasis on Spheroidal Graphite Cast Irons, *Metals* (Basel). 12 (2022) 1–80. <https://doi.org/10.3390/met12030504>.
- [8] A.F. Society, *Mold & Core Test Handbook*, American Foundry Society, (2001).
- [9] J. Campbell, *Molds and cores*, 2011. <https://doi.org/10.1016/b978-1-85617-809-9.10004-0>.
- [10] P. Scarber, C.E. Bates, J. Griffin, Effects of Mold and Binder Formulations on Gas Evolution When Pouring Aluminum Castings, *Trans. Am. Foundry Soc.* 114 (2006) 1–11.
- [11] L. Winardi, *Procedures for Predicting Pressures inside Cores*, (2007).
- [12] Winardi, L., Griffin, R. D., Littleton, H. E. & Griffin, J. A. Variables Affecting Gas Evolution Rates and Volumes from Cores in Contact with Molten Metal. *Trans. Am. Foundry Soc.* (2008) 116, 1–18.
- [13] J. Campbell, *Molding and Casting Processes*, *Cast Iron Sci. Technol.* 1 (2018) 189–206. <https://doi.org/10.31399/asm.hb.v01a.a0006297>.
- [14] *Green Sand Molding, Casting, Vol 15, ASM Handbook*, Edited By Srinath Viswanathan, Diran Apelian, Raymond J. Donahue, Babu DasGupta, Michael Gywn, John L. Jorstad, Raymond W. Monroe, Mahi Sahoo, Thomas E. Prucha, Daniel Twarog, ASM International, (2008), p 549–566, <https://doi.org/10.31399/asm.hb.v15.a0005243>

- [15] Chemically bonded molds & cores: An operator's manual for the use of chemically bonded sand mixtures., American Foundrymen's Society, Des plaines, Illinois, (1987).
- [16] Coremaking, *Casting*, Vol 15, *ASM Handbook*, Edited By Srinath Viswanathan, Diran Apelian, Raymond J. Donahue, Babu DasGupta, Michael Gywn, John L. Jorstad, Raymond W. Monroe, Mahi Sahoo, Thomas E. Prucha, Daniel Twarog, ASM International, (2008), p 581–597, <https://doi.org/10.31399/asm.hb.v15.a0005244>
- [17] No-Bake Sand Molding, *Casting*, Vol 15, *ASM Handbook*, Edited By Srinath Viswanathan, Diran Apelian, Raymond J. Donahue, Babu DasGupta, Michael Gywn, John L. Jorstad, Raymond W. Monroe, Mahi Sahoo, Thomas E. Prucha, Daniel Twarog, ASM International, (2008), p 567–580, <https://doi.org/10.31399/asm.hb.v15.a0005354>
- [18] D.A. Nield, A. Bejan, *Convection in porous media: Fourth edition*, (2012). <https://doi.org/10.1007/978-1-4614-5541-7>.
- [19] J. Jorstad, M.B. Krusiak, J.O. Serra, V. La Fay, *Aggregates and Binders for Expendable Molds*, *Casting* (2018) 528–548. <https://doi.org/10.31399/asm.hb.v15.a0005242>.
- [20] J. Svidr6, A. Di6szegi, J.T. Svidr6, The origin of thermal expansion differences in various size fractions of silica sand, *Int. J. Cast Met. Res.* 33 (2020) 242–249. <https://doi.org/10.1080/13640461.2020.1838078>.
- [21] Merkus, Henk G. *Particle size measurements: fundamentals, practice, quality*. Vol. 17. (2009). Springer Science & Business Media,
- [22] J.E. Houghton, J. Behnsen, R.A. Duller, T.E. Nichols, R.H. Worden, Particle size analysis: A comparison of laboratory-based techniques and their application to geoscience, *Sediment. Geol.* 464 (2024) 106607. <https://doi.org/10.1016/j.sedgeo.2024.106607>.
- [23] J.G. Behnsen, K. Black, J.E. Houghton, R.H. Worden, A Review of Particle Size Analysis with X-ray CT, *Materials (Basel)*. 16 (2023) 1–17. <https://doi.org/10.3390/ma16031259>.
- [24] A.H. Lefebvre, V.G. McDonell, *Atomization and sprays*, CRC press, (2017).
- [25] A.D. SARKAR, Sand Testing, *Mould Core Mater. Steel Foundry* (1967) 5–19. <https://doi.org/10.1016/b978-0-08-012486-5.50005-0>.
- [26] P.J. Lloyd, Particle Characterization., *Chem. Eng. (New York)* 81 (1974) 120–123. <https://doi.org/10.1201/9781315141381-2>.
- [27] M.N. Pons, J. Dodds, *Particle Shape Characterization by Image Analysis*, Elsevier Ltd, (2015). <https://doi.org/10.1016/B978-0-12-384746-1.00015-X>.
- [28] U. Ulusoy, Quantifying of particle shape differences of differently milled barite

- using a novel technique: Dynamic image analysis, *Materialia* 8 (2019).
<https://doi.org/10.1016/j.mtla.2019.100434>.
- [29] J.R. Brown, *Foseco Ferrous Foundryman 's Handbook Foseco Ferrous Foundryman 's Handbook Edited by, (2000) 1–352.*
- [30] M. Holtzer, R. Dańko, A. Kmita, D. Drożyński, M. Kubecki, M. Skrzyński, A. Roczniak, Environmental impact of the reclaimed sand addition to molding sand with furan and phenol-formaldehyde resin—a comparison, *Materials (Basel)*. 13 (2020) 1–12. <https://doi.org/10.3390/ma13194395>.
- [31] R. CHEN, Y. KIRSH, *Thermogravimetry, Differential Thermal Analysis and Associated Methods, Anal. Therm. Stimul. Process. (1981) 82–122.*
<https://doi.org/10.1016/b978-0-08-022930-0.50010-4>.
- [32] B. Grabowska, P. Malinowski, M. Szucki, Ł. Byczyński, Thermal analysis in foundry technology: Part 1. Study TG–DSC of the new class of polymer binders BioCo, *J. Therm. Anal. Calorim.* 126 (2016) 245–250. <https://doi.org/10.1007/s10973-016-5435-5>.
- [33] B. Grabowska, S. Żymankowska-Kumon, S. Cukrowicz, K. Kaczmarska, A. Bobrowski, B. Tyliczszak, Thermoanalytical tests (TG–DTG–DSC, Py-GC/MS) of foundry binders on the example of polymer composition of poly(acrylic acid)–sodium carboxymethylcellulose, *J. Therm. Anal. Calorim.* 138 (2019) 4427–4436. <https://doi.org/10.1007/s10973-019-08883-5>.
- [34] B. Grabowska, K. Hodor, K. Kaczmarska, A. Bobrowski, Ż. Kurleto-Kozioł, C. Fischer, Thermal analysis in foundry technology: Part 2. TG–DTG–DSC, TG–MS and TG–IR study of the new class of polymer binders BioCo, *J. Therm. Anal. Calorim.* 130 (2017) 301–309. <https://doi.org/10.1007/s10973-017-6506-y>.
- [35] J. Zych, J. Mocek, N. Kaźnica, Kinetics of gases emission from surface layers of sand moulds, *Arch. Foundry Eng.* 18 (2018) 222–226.
<https://doi.org/10.24425/118841>.
- [36] G. Jomaa, P. Goblet, C. Coquelet, V. Morlot, Kinetic modeling of polyurethane pyrolysis using non-isothermal thermogravimetric analysis, *Thermochim. Acta* 612 (2015) 10–18. <https://doi.org/10.1016/j.tca.2015.05.009>.
- [37] M.M. Mashingaidze, Curing properties of Furotec 132 resin-bonded foundry sand, *Arch. Foundry Eng.* 19 (2019) 117–123.
<https://doi.org/10.24425/afe.2019.129641>.
- [38] S.G. Acharya, J.A. Vadher, P. V. Kanjariya, Identification and Quantification of Gases Releasing from Furan No Bake Binder, *Arch. Foundry Eng.* 16 (2016) 5–10.
<https://doi.org/10.1515/afe-2016-0039>.
- [39] P. Wan, J. Zhou, Y. Li, Y. Yin, X. Peng, X. Ji, X. Shen, Kinetic analysis of resin binder for casting in combustion decomposition process, *J. Therm. Anal. Calorim.* (2021).
<https://doi.org/10.1007/s10973-021-10902-3>.

- [40] A. Kmita, W. Knauer, M. Holtzer, K. Hodor, G. Piwowarski, A. Roczniak, K. Górecki, The decomposition process and kinetic analysis of commercial binder based on phenol-formaldehyde resin, using in metal casting, *Appl. Therm. Eng.* 156 (2019) 263–275. <https://doi.org/10.1016/j.applthermaleng.2019.03.093>.
- [41] H. Wolff, S. Engler, A. Schrey, G. Wolf, Thermophysical properties of mold materials, *Adv. Eng. Mater.* 5 (2003) 55–58. <https://doi.org/10.1002/adem.200390008>.
- [42] M. Holtzer, A. Kmita, *Mold and Core Sands in Metalcasting: Chemistry and Ecology*, (2020). <https://doi.org/10.1007/978-3-030-53210-9>.
- [43] Y. Wang, H. Huang, F.S. Cannon, R.C. Voigt, S. Komarneni, J.C. Furness, Evaluation of volatile hydrocarbon emission characteristics of carbonaceous additives in green sand foundries, *Environ. Sci. Technol.* 41 (2007) 2957–2963. <https://doi.org/10.1021/es0628295>.
- [44] C.E. Bates, M. RW, *Mold binder decomposition and its relation to gas defects in castings*, (1981).
- [45] Winardi, L., Littleton, H. E. & Bates, C. E. Gas Pressures in Sand Cores. *Trans. Am. Foundry Soc.* (2007) 115, 1–10.
- [46] L. Winardi, H.E. Littleton, C.E. Bates, Gas Pressures in Sand Cores, *Trans. Am. Foundry Soc.* 115 (2007) 1–10.
- [47] C.E. Bates, W.D. Scott, Decomposition of resin binders and the relationship between the gases formed and the casting surface quality–Part 2. Gray iron, *Trans. Am. Foundrymen’s Soc.* 84 (1977) 793–804.
- [48] G. Samuels, C. Beckermann, Measurement of gas evolution from PUNB bonded sand as a function of temperature, *Int. J. Met.* 6 (2012) 23–40. <https://doi.org/10.1007/BF03355525>.
- [49] R. Monroe, Porosity in Castings, *ChemInform* 37 (2006) 1–28. <https://doi.org/10.1002/chin.200642218>.
- [50] L. Mádi, I. Budavári, L. Varga, The effect of different grain sizes and heat input on the gas pressure inside artificial resin-bonded sand cores, *IOP Conf. Ser. Mater. Sci. Eng.* 903 (2020). <https://doi.org/10.1088/1757-899X/903/1/012034>.
- [51] J. Campbell, *The 10 Rules for good castings*, 2011. <https://doi.org/10.1016/b978-1-85617-809-9.10010-6>.
- [52] B. Kirchebner, S. Kammerloher, G. Fuchs, E. Reberger, W. Volk, P. Lechner, A Test Stand for Quantifying the Core Gas Release and the Gas Permeability of Inorganically-Bound Foundry Cores, *Int. J. Met.* (2023). <https://doi.org/10.1007/s40962-023-01090-x>.
- [53] R.G. Swanson, Porosity and Permeability, *Sample Exam. Man.* (2020) 16–18. <https://doi.org/10.1306/mth1413c5>.

- [54] S.P. Neuman, Theoretical derivation of Darcy's law, *Acta Mech.* 25 (1977) 153–170. <https://doi.org/10.1007/BF01376989>.
- [55] J. Zych, J. Kolczyk, T. Snopkiewicz, New Investigation Method of the Permeability of Ceramic Moulds Applied in the Investment Casting Technology, *Arch. Foundry Eng.* 13 (2013) 107–112. <https://doi.org/10.2478/afe-2013-0047>.
- [56] S. Paż, D. Drożyński, M. Górny, S. Cukrowicz, Properties of Bentonites and Bentonite Mixtures used in Casting Processes, *Arch. Foundry Eng.* 19 (2019) 35–40. <https://doi.org/10.24425/afe.2019.127113>.
- [57] Winardi, L.; Littleton, H.; Bates, C.E. New Technique for Measuring Permeability of Cores Made from Various Sands, Binders, Additives and Coatings. *Trans. Am. Foundry Soc.* (2005), 113, 393–406..
- [58] <https://www.multiserw-morek.pl>.
- [59] S. Kumar, D.B. Karunakar, Enhancing the Permeability and Properties of Ceramic Shell in Investment Casting Process Using ABS Powder and Needle Coke, *Int. J. Met.* 13 (2019) 588–596. <https://doi.org/10.1007/s40962-018-00297-7>.
- [60] S. Mitra, M. EL Mansori, A. Rodríguez de Castro, M. Costin, Study of the evolution of transport properties induced by additive processing sand mold using X-ray computed tomography, *J. Mater. Process. Technol.* 277 (2020) 116495. <https://doi.org/10.1016/j.jmatprotec.2019.116495>.
- [61] F. Ettemeyer, P. Lechner, T. Hofmann, H. Andrä, M. Schneider, D. Grund, W. Volk, D. Günther, Digital sand core physics: Predicting physical properties of sand cores by simulations on digital microstructures, *Int. J. Solids Struct.* 188–189 (2020) 155–168. <https://doi.org/10.1016/j.ijsolstr.2019.09.014>.
- [62] L. Mádi, L. Varga, The effect of gas permeability on the pressure of artificial resin-bonded core gases, *IOP Conf. Ser. Mater. Sci. Eng.* 426 (2018). <https://doi.org/10.1088/1757-899X/426/1/012033>.
- [63] P.A. Scholle, Porosity, *A Color Illus. Guid. To Const. Textures, Cem. Porosities Sandstones Assoc. Rocks V* (2020) 169–181. <https://doi.org/10.1306/m28402c12>.
- [64] A.E. SCHEIDEGGER, *the Physics of Flow Through Porous Media*, (1974). <https://doi.org/10.1097/00010694-195812000-00015>.
- [65] H. Hudák, L. Varga, Examination of correlation between the granulometric properties of molding and core sand mixtures and their production parameters, *IOP Conf. Ser. Mater. Sci. Eng.* 903 (2020). <https://doi.org/10.1088/1757-899X/903/1/012060>.
- [66] B. Marks, B. Sandnes, G. Dumazer, J.A. Eriksen, K.J. Måløy, Compaction of granular material inside confined geometries, *Front. Phys.* 3 (2015) 1–9. <https://doi.org/10.3389/fphy.2015.00041>.

- [67] A. Costa, Permeability-porosity relationship: A reexamination of the Kozeny-Carman equation based on a fractal pore-space geometry assumption, *Geophys. Res. Lett.* 33 (2006) 1–5. <https://doi.org/10.1029/2005GL025134>.
- [68] L.M. Anovitz, D.R. Cole, Characterization and analysis of porosity and pore structures, *Pore Scale Geochemical Process.* (2015) 61–164. <https://doi.org/10.2138/rmg.2015.80.04>.
- [69] M.T.Q.S. da Silva, F. Perretto, M. do Rocio Cardoso, W. Mazer, Porosity: Some characterization techniques, *Mater. Today Proc.* (2023). <https://doi.org/10.1016/j.matpr.2023.03.716>.
- [70] T. Lever, P. Haines, J. Rouquerol, E.L. Charsley, P. Van Eckeren, D.J. Burlett, IUPAC nomenclature of thermal analysis (IUPAC Recommendations 2014), *Pure Appl. Chem.* 86 (2014) 545–553. <https://doi.org/10.1515/pac-2012-0609>.
- [71] J. Van Keulen, Density of porous solids, *Matériaux Constr.* 6 (1973) 181–183. <https://doi.org/10.1007/BF02479031>.
- [72] G. V Chilingarian, K.H. Wolf, D.R.B.T.-D. in S. Allen, Chapter 1 Introduction, in: *Compact. Coarse-Grained Sediments*, Elsevier, 1975: pp. 1–42. [https://doi.org/https://doi.org/10.1016/S0070-4571\(08\)71083-5](https://doi.org/https://doi.org/10.1016/S0070-4571(08)71083-5).
- [73] B. Ghanbarian, F. Male, Theoretical power-law relationship between permeability and formation factor, *J. Pet. Sci. Eng.* 198 (2021) 108249. <https://doi.org/10.1016/j.petrol.2020.108249>.
- [74] C.H. Shin, Permeability variation analysis using the superficial diameter correlation with porosity change, *Phys. Fluids* 33 (2021). <https://doi.org/10.1063/5.0050301>.
- [75] T.J. MARSHALL, a Relation Between Permeability and Size Distribution of Pores, *J. Soil Sci.* 9 (1958) 1–8. <https://doi.org/10.1111/j.1365-2389.1958.tb01892.x>.
- [76] S. Lowell, J.E. Shields, M.A. Thomas, M. Thommes, Mercury Porosimetry: Non-wetting Liquid Penetration, (2004) 157–188. https://doi.org/10.1007/978-1-4020-2303-3_10.
- [77] T. Sivarupan, M. El Mansori, K. Daly, M.N. Mavrogordato, F. Pierron, Characterisation of 3D printed sand moulds using micro-focus X-ray computed tomography, *Rapid Prototyp. J.* 25 (2019) 404–416. <https://doi.org/10.1108/RPJ-04-2018-0091>.
- [78] D. Martinez, C. Bate, G. Manogharan, Towards Functionally Graded Sand Molds for Metal Casting: Engineering Thermo-mechanical Properties Using 3D Sand Printing, *Jom* 72 (2020) 1340–1354. <https://doi.org/10.1007/s11837-019-03975-x>.
- [79] J. Zhu, R. Zhang, Y. Zhang, F. He, The fractal characteristics of pore size distribution in cement-based materials and its effect on gas permeability, *Sci. Rep.* 9 (2019) 1–12. <https://doi.org/10.1038/s41598-019-53828-5>.

- [80] N. Nishiyama, T. Yokoyama, Permeability of porous media: Role of the critical pore size, *J. Geophys. Res. Solid Earth* 122 (2017) 6955–6971.
<https://doi.org/10.1002/2016JB013793>.
- [81] A.J. Katz, A.H. Thompson, Quantitative prediction of permeability in porous rock, *Phys. Rev. B* 34 (1986) 8179.
- [82] K.M. Graczyk, M. Matyka, Predicting porosity, permeability, and tortuosity of porous media from images by deep learning, *Sci. Rep.* 10 (2020) 1–11.
<https://doi.org/10.1038/s41598-020-78415-x>.
- [83] P.W.J. Glover, E. Walker, Grain-size to effective pore-size transformation derived from electrokinetic theory, *Geophysics* 74 (2009).
<https://doi.org/10.1190/1.3033217>.
- [84] C.T. Davie, C.J. Pearce, N. Bićanić, Aspects of Permeability in Modelling of Concrete Exposed to High Temperatures, *Transp. Porous Media* 95 (2012) 627–646.
<https://doi.org/10.1007/s11242-012-0066-1>.
- [85] D.R. Faulkner, E.H. Rutter, The effect of temperature, the nature of the pore fluid, and subyield differential stress on the permeability of phyllosilicate-rich fault gouge, *J. Geophys. Res. Solid Earth* 108 (2003) 1–12.
<https://doi.org/10.1029/2001jb001581>.
- [86] M. Rödning, Z. Ma, S. Torquato, Predicting permeability via statistical learning on higher-order microstructural information, *Sci. Rep.* 10 (2020) 1–17.
<https://doi.org/10.1038/s41598-020-72085-5>.
- [87] A.E. Scheidegger, *The physics of flow through porous media*, University of Toronto press, (1957).
- [88] K.M. Sundaram, Permeability of unimodal pore system, (2022).
<https://doi.org/10.1016/B978-0-444-64169-4.00011-0>.
- [89] J. Happel, Viscous flow in multiparticle systems: Slow motion of fluids relative to beds of spherical particles, *AIChE J.* 4 (1958) 197–201.
<https://doi.org/10.1002/aic.690040214>.
- [90] C.F. Berg, Permeability Description by Characteristic Length, Tortuosity, Constriction and Porosity, *Transp. Porous Media* 103 (2014) 381–400.
<https://doi.org/10.1007/s11242-014-0307-6>.
- [91] A. Starobin, C.W. Hirt, D. Goettsch, A model for binder gas generation and transport in sand cores and molds, *Proc. from 12th Int. Conf. Model. Cast. Welding, Adv. Solidif. Process.* (2009) 345–352.
- [92] J. Thorborg, S. Kumar, I. Wagner, J.C. Sturm, The virtual core - Modelling and optimization of core manufacturing and application, *IOP Conf. Ser. Mater. Sci. Eng.* 861 (2020). <https://doi.org/10.1088/1757-899X/861/1/012004>.
- [93] A. Dioszegi, E. Dioszegi, J. Toth, J.T. Svidro, Modelling and simulation of heat

- conduction in 1-D polar spherical coordinates using control volume-based finite difference method, *Int. J. Numer. Methods Heat Fluid Flow* 26 (2016) 2–17. <https://doi.org/10.1108/HFF-10-2014-0318>.
- [94] K. Kubo, R.D. Pehlke, Heat and moisture transfer in sand molds containing water, *Metall. Trans. B* 17 (1986) 903–911. <https://doi.org/10.1007/BF02657153>.
- [95] J.T. Svidró, A. Diószegi, J. Svidró, T. Ferenczi, The effect of different binder levels on the heat absorption capacity of moulding mixtures made by the phenolic urethane cold-box process, *J. Therm. Anal. Calorim.* 130 (2017) 1769–1777. <https://doi.org/10.1007/s10973-017-6611-y>.
- [96] A. Kmita, W. Knauer, M. Holtzer, K. Hodor, G. Piwowarski, A. Roczniak, K. Górecki, The decomposition process and kinetic analysis of commercial binder based on phenol-formaldehyde resin, using in metal casting, *Appl. Therm. Eng.* 156 (2019) 263–275. <https://doi.org/10.1016/j.applthermaleng.2019.03.093>.
- [97] M. Monti, H. Hoydonckx, F. Stappers, G. Camino, Thermal and combustion behavior of furan resin/silica nanocomposites, *Eur. Polym. J.* 67 (2015) 561–569. <https://doi.org/10.1016/j.eurpolymj.2015.02.005>.
- [98] T. Ozawa, A modified method for kinetic analysis of thermoanalytical data, *J. Therm. Anal.* 9 (1976) 369–373. <https://doi.org/10.1007/BF01909401>.
- [99] G. R. Heal, in *Principles of Thermal Analysis and Calorimetry*, ed. P. Haines, The Royal Society of Chemistry, (2002), pp. 10-54.
- [100] Thermogravimetric Analysis, *Materials Characterization*, Vol 10, ed., *ASM Handbook*, ASM International, (2019), p 312–318, <https://doi.org/10.31399/asm.hb.v10.a0006673>
- [101] <https://www.magma-soft.de/en/solutions/magma-soft/>.
- [102] S.O. Hansson, The art of doing science, *Dep. Philos. Hist.* (2007).
- [103] T. Grüne-Yanoff, *Experiments Models & Methodology Theory and Methodology of Science-Course Text*, (2021).
- [104] K. Säfsten, M. Gustavsson, *Research methodology: for engineers and other problem-solvers*, (2020). Retrieved from <https://urn.kb.se/resolve?urn=urn:nbn:se:hj:diva-51270>
- [105] J. Tóth, J.T. Svidró, A. Diószegi, D. Stevenson, Heat absorption capacity and binder degradation characteristics of 3D printed cores investigated by inverse fourier thermal analysis, *Int. J. Met.* 10 (2016) 276–288. <https://doi.org/10.1007/s40962-016-0043-5>.
- [106] B. Esteban, J.R. Riba, G. Baquero, A. Rius, R. Puig, Temperature dependence of density and viscosity of vegetable oils, *Biomass and Bioenergy* 42 (2012) 164–171. <https://doi.org/10.1016/j.biombioe.2012.03.007>.

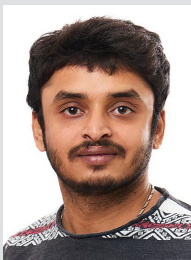
- [107] E.N. Landis, D.T. Keane, X-ray microtomography, *Mater. Charact.* 61 (2010) 1305–1316. <https://doi.org/10.1016/j.matchar.2010.09.012>.
- [108] J. Schindelin, I. Arganda-Carreras, E. Frise, V. Kaynig, M. Longair, T. Pietzsch, S. Preibisch, C. Rueden, S. Saalfeld, B. Schmid, J.-Y. Tinevez, D.J. White, V. Hartenstein, K. Eliceiri, P. Tomancak, A. Cardona, Fiji: an open-source platform for biological-image analysis, *Nat. Methods* 9 (2012) 676–682. <https://doi.org/10.1038/nmeth.2019>.
- [109] E. Baril, The Permeability of Metal Foams and its Dependence on Microstructure, (2005). Concordia university.
- [110] X. Wang, Q. Wu, Y. Huang, N. Li, X. Wu, X. Chen, J. Wang, T. Jing, T. Huang, J. Kang, Study on the Gas Release of 3D-Printed Furan Resin Sand Core during the Casting Process, *Materials (Basel)*. 16 (2023) 1–15. <https://doi.org/10.3390/ma16114152>.
- [111] A. Diószegi, J. Hattel, Inverse thermal analysis method to study solidification in cast iron, *Int. J. Cast Met. Res.* 17 (2004) 311–318. <https://doi.org/10.1179/136404604225020687>.
- [112] J.T. Svidró, A. Diószegi, J. Tóth, The novel application of Fourier thermal analysis in foundry technologies: Examination of degradation characteristics in resin-bound moulding materials, *J. Therm. Anal. Calorim.* 115 (2014) 331–338. <https://doi.org/10.1007/s10973-013-3289-7>.
- [113] T. Ozawa, A New Method of Quantitative Differential Thermal Analysis, *Bull. Chem. Soc. Jpn.* 39 (1966) 2071–2085. <https://doi.org/10.1246/bcsj.39.2071>.

Gas Evolution and Transport in Foundry Sands

Sand-casting is one of the most widely used cost-effective manufacturing techniques to produce metal components for various industries. Constantly evolving environmental regulations have increased the necessity for circular and sustainable manufacturing practices. During the casting process, the mold and core undergo a thermal shock when they come in contact with the molten metal. This triggers a severe reaction due to the evaporation of volatiles and the decomposition of chemical binders. When the generated gases are not evacuated efficiently, they affect the cast component by aiding in defect formation.

In this work, the phenomena that affect heat and mass transport due to the generated gases are studied with the help of newly developed experimental techniques in combination with porous material characterization tools. Combining the experimental data with thermal analysis techniques, a computational model for the heat and mass transport in the foundry core is also developed. A custom-made measurement setup to measure the permeability of molds and cores is presented. Using the setup, the effect of variation in the grain size distribution and the density on the permeability is quantified. Also, a novel method to quantify the gases generated from foundry sand mixtures where the core/mold is subjected to conditions similar to the actual casting process is presented. Along with accurate gas volume data, simultaneous temperature measurements in the central and lateral parts of the sample enabled accurate estimation of the heat absorption characteristics associated with the binder decomposition and the gas generation. Additionally, thermogravimetry analysis was performed for the Furan binder with several heating rates to study the decomposition characteristics and kinetics. Using the obtained gas transport properties and the kinetic parameters of the binder decomposition and assuming a local thermal non-equilibrium model for heat transport in the porous material, a computational model was developed for the gas generation and transport process in foundry sand cores/molds.

By studying the gas evolution and transport phenomena and developing accurate computational models for heat and gas transport in foundry sands, the work presented in this thesis helps reduce the defects formed due to the gas generation phenomenon, aiding sustainable manufacturing of cast components.



DINESH SUNDARAM is currently a doctoral candidate in the Materials and Manufacturing department at Jönköping University. He holds a bachelor's degree in Mechanical engineering from SASTRA University, India. His M.Sc. degree in Material Science and Engineering from the Royal Institute of Technology (KTH, university) focussed on Materials Design. He has been working in the field of Foundry Technology for his Doctoral degree. His research interests are in the fields of metallurgy, porous materials, heat and mass transport, and foundry technology.

ISBN 978-91-89785-11-3 (Printed version)

ISBN 978-91-89785-12-0 (Online version)